

An extremely luminous panchromatic outburst from the nucleus of a distant galaxy

A. J. Levan,^{1*} N. R. Tanvir,² S. B. Cenko,³ D. A. Perley,³ K. Wiersema,² J. S. Bloom,³ A. S. Fruchter,⁴ A. de Ugarte Postigo,⁵ P. T. O'Brien,² N. Butler,^{3,6} A. J. van der Horst,⁷ G. Leloudas,⁵ A. N. Morgan,³ K. Misra,⁴ G. C. Bower,³ J. Farihi,² R. L. Tunnicliffe,¹ M. Modjaz,^{3,8} J. M. Silverman,³ J. Hjorth,⁵ C. Thöne,⁹ A. Cucchiara,³ J. M. Castro Cerón,¹⁰ A.J. Castro-Tirado,⁹ J. A. Arnold,¹¹ M. Bremer,¹² J. P. Brodie,¹¹ T. Carroll,¹³ M. C. Cooper,^{14,15} P. A. Curran,¹⁶ R. M. Cutri,¹⁷ J. Ehle,¹³ , D. Forbes,¹⁸ J. Fynbo,⁵ J. Gorosabel,⁹ J. Graham,^{4,29} S. Guziy,⁹ D. I. Hoffman,¹⁹ P. Jakobsson,²⁰ A. Kamble,²¹ T. Kerr,¹³ M. M. Kasliwal,¹⁹ C. Kouveliotou,²² D. Kocsevki,¹¹ N. M. Law,²² P. E. Nugent,²³ E. O. Ofek,¹⁹ D. Poznanski,^{3,6,23} R. M. Quimby,¹⁹ E. Rol,²⁴ A. J. Romanowsky,¹¹ R. Sánchez-Ramírez,⁹ S. Schulze,²⁰ N. Singh,¹¹ R. L. C. Starling,² R. G. Strom,²⁷ P. J. Wheatley,¹ R. A. M. J. Wijers,²⁶ J. M. Winters,²⁷ T. Wold,¹³ D. Xu²⁸

*To whom correspondence should be addressed; E-mail: a.j.levan@warwick.ac.uk

Variable X-ray and γ -ray emission is characteristic of the most extreme physical processes in the Universe, and studying the sources of these energetic photons has been a major driver in astronomy for the past 50 years. Here we present multiwavelength observations of a unique γ -ray selected transient, discovered by Swift, which was accompanied by bright emission across the electromagnetic spectrum, and whose properties are unlike any previously observed source. We pinpoint the event to the center of a small, star-forming galaxy at redshift $z = 0.3534$. Its high-energy emission has lasted much longer than any gamma-ray burst, while its peak luminosity was ~ 100 times higher than bright active galactic nuclei. The association of the outburst with the cen-

ter of its host galaxy suggests that this phenomenon has its origin in a new, rare mechanism associated with a massive black hole in the nucleus of a galaxy

Surveys of the sky at short wavelengths (X-ray and γ -ray) reveal a much more dynamic Universe than seen at optical wavelengths. Many sources vary substantially, and the most extreme transform from invisibility to the brightest objects in the sky, sometimes on timescales of seconds. The sources of such bursts of high-energy radiation have proven difficult to trace, but coherent observational programmes have shown that some fraction originate in the Milky Way, either from isolated neutron stars with intense magnetic fields (1), or from binary systems containing neutron stars and black holes (2). Some, long lived, but variable X- and γ -ray emission originates in active galaxies (3), while the brightest and perhaps most spectacular class are the long-duration gamma-ray bursts (long-GRBs) which are detected at a rate of ~ 2 per week by current missions such as the *Swift* satellite (4), and are now thought to originate from the collapse of massive stars in the distant Universe (5, 6).

In this paper we present observations, spanning radio to γ -ray, of a new type of transient, GRB 110328A/*Swift* J164449.3+573451, hereafter Sw 1644+57. It is more luminous than any active galaxy, yet longer lived than any long-GRB. It defies placement into any of the classes of object described above, and suggests a new channel for the creation of highly energetic transient events.

Sw 1644+57 was first detected by the *Swift* Burst Alert Telescope (BAT) at 12:57:45 UT on 28 March 2011 (10). It was characterized as a long image trigger, with a low count rate (not sufficient to trigger the instrument) but a duration of > 1000 s, allowing a point source to be recovered in the image plane. *Swift* follow-up observations with the Ultraviolet and Optical Telescope (UVOT) and X-ray Telescope (XRT) only began 1475 s after the initial outburst. No source was seen in the UVOT observations, but a bright point source was found with the XRT (10). Unlike any previously observed long-GRB (which typically decline substantially

on a timescale of minutes), it remained bright and highly variable for a prolonged period, and went on to re-trigger the BAT on three further occasions over the next 48 hours (49). Re-examination of previous γ -ray observations of this region showed that the source appears to have been present a few days before the initial trigger, but not at earlier times (9). Equally unlike any normal long-GRB, the source remained bright in the X-rays for more than two weeks (see Figure 1). The early X-ray behaviour showed the same dramatic flaring seen by BAT, with flares having time-scales of hours, and with broadly similar shapes. After the first 48 hours the X-rays maintained a more constant level, albeit with episodic brightening and fading spanning more than an order of magnitude in flux.

Our first ground based observations of Sw 1644+57 began approximately two hours after the burst trigger, with the Gemini-North Telescope in Hawaii. Unfortunately, poor weather conditions meant that only shallow observations were possible, and these did not yield any candidate optical counterpart to a limit of $r \sim 22.1$. At 13 hours post-trigger we obtained imaging with the Nordic Optical Telescope (NOT) on La Palma, which revealed a $R = 22.5$ magnitude source consistent with the X-ray localisation (11). Our examination of archival images obtained with the Palomar Transient Factory (PTF) revealed this source to be present at approximately the same brightness more than a year prior to the outburst, and indeed our subsequent optical monitoring (below) confirms the optical flux is dominated by the host galaxy. Early analysis of the X-ray/ γ -ray data was used to argue that the transient was most likely a source within the Milky Way (12). However, our spectroscopy of the optical counterpart with Gemini-North (13), the Gran Telescopio Canarias (GTC) in La Palma (14), and the Keck Telescope in Hawaii (15) showed strong emission lines of hydrogen and oxygen (as well as absorption lines from a moderate age stellar population), consistent with a star-forming galaxy at a systemic redshift of $z = 0.3534 \pm 0.0002$ (see Figure 2). Thus we concluded Sw 1644+57 was a source at cosmological distance with extremely unusual properties, and this sparked a

global follow-up campaign in an effort to elucidate its nature.

We continued to monitor the field from the ground in the optical and near infrared (nIR) with Gemini-North, the United Kingdom Infrared Telescope (UKIRT), NOT, PAIRITEL and GTC, obtaining observations from the *B*-band (435 nm) to the *L*-band (3780 nm). In contrast to the non-varying behaviour in the optical, these data showed that at nIR wavelengths the source fluctuated by more than a factor of 3 in flux over several days, indicating that the γ -ray transient was also producing considerable longer-wavelength emission. Our detection in the *L*-band ($270 \pm 50 \mu\text{Jy}$) at a level more than an order of magnitude above our limit from *WISE* on any quiescent emission from the host galaxy at $3.4 \mu\text{m}$ emphasises this point (16). The infrared variations roughly track those of the X-ray (see Figure 1), but are certainly not perfectly correlated, suggesting multiple emission components.

We triggered a target of opportunity observation with the *Chandra X-ray Observatory*, which took place about 6.5 days after the initial outburst. This confirmed that the X-ray lightcurve is frequently highly variable on timescales of seconds (Figure 1). Specifically our *Chandra* observations show that factor of 2 changes in flux continued to occur on ~ 100 s even at comparatively late times. However, our photometry of individual optical and nIR images (with a time resolution of 20–60 s) does not reveal rapid variability in the nIR light. In the optical *r*-band little variability was seen ($< 10\%$) on all time-scales, indicating that the host galaxy dominates the optical emission. We conclude that the transient has a very red optical-nIR colour, which may be due to a high dust column along the line of sight. The dust hypothesis would be consistent with the high hydrogen column density inferred from the X-ray spectrum (10^{22} cm^{-2}), which implies host extinction of $A_V \sim 6$ (17) and together these findings suggest that the source is situated in a dense and dusty region, such as a galactic nucleus (see Supplementary Online Material for more information).

Observations at still longer wavelengths showed a bright radio (18), and millimeter source

(19) at the same location. Our millimeter observations from IRAM confirm this, and radio (1.4. and 4.8 GHz) observations from Westerbork Synthesis Radio Telescope (WSRT) show a bright source, which brightened over the first week following the outburst (Figure 1, lower panel). These observations demonstrate that Sw 1644+57 was emitting strong radiation across the electromagnetic spectrum.

The character of the host galaxy and the position of the transient within it are potentially important clues to the nature of Sw 1644+57, and to this end, we obtained observations with the *Hubble Space Telescope* on 4 April 2011. In the nIR the image remains unresolved, consistent with emission from the transient still dominating, but in the optical wavebands we clearly detect the light of the host galaxy. The WFC3 IR position of the transient falls within 0.03 arcseconds (1σ , < 150 pc at $z = 0.3534$) of the center of the host galaxy (see Figure 3). We additionally obtained VLBA observations of Sw 1644+57 on 1 April 2011, providing another precise astrometric position, with an offset from the center of the host of 0.04 ± 0.07 arcseconds, further strengthening the association with the nucleus of the host [see also (20)].

The host galaxy itself appears compact, and non-interacting, with a half-light radius in the optical of $r_h = 1.04$ kpc, and an absolute magnitude of $M_V = -18.19$ (comparable in luminosity to the Large Magellanic Cloud). Subtraction of a point source from the *HST* F606W image suggests an upper limit to the transient magnitude in that band of 30% of the host light, or a magnitude of 24.1 (AB). The measured ratios of emission lines are consistent with them originating from a normal star forming galaxy that has not, at least until now, contained an active nucleus. The inferred star formation rate of the host is $0.5 M_\odot \text{ yr}^{-1}$.

Our observations clearly show that the transient originates from the center of a galaxy at cosmological distances. At this redshift (which corresponds to a luminosity distance $d_L = 1.81$ Gpc, assuming $H_0 = 73 \text{ km s}^{-1} \text{ Mpc}^{-1}$, $\Omega_\Lambda = 0.73$, $\Omega_M = 0.27$), the the brightest X-ray flare reached a luminosity of $L_X \sim 3 \times 10^{48} \text{ erg s}^{-1}$ (isotropic equivalent) for ~ 1000 s.

The total energy output in the first $\sim 10^6$ s after outburst of $\sim 10^{53}$ erg, is equivalent to $\sim 10\%$ of the rest energy of the Sun. While these numbers are not abnormal for long-duration GRBs, the properties of this outburst are clearly distinct from the long-GRB population. First, the repetition of the γ -ray trigger 4 times in 48 hours is unheard of for long-GRBs, which are destructive, and non-repeating events. Further, the duration of bright X-ray emission is much longer than has ever been seen for any long-GRB [e.g., (21, 22)], persisting at $L_X \sim 10^{47}$ erg s $^{-1}$ two weeks after the initial event. This, together with the origin in the core of its host galaxy, lead us to infer that Sw 1644+57 most likely originates from the central massive black hole. However, the X-ray luminosity of Sw 1644+57 is well beyond the bright end of the quasar luminosity function (23), and is more luminous (by a factor of ~ 100) than flares from the brightest blazars [e.g., (3)]. Interestingly, though, its optical luminosity is a factor of $\sim 10^4$ fainter than a bright QSO [e.g., (24)], implying either differing emission processes or (as in fact seems to be the case from the red colour) a particularly high dust column within the host. The overall energetics and long-duration, together with the order-of-magnitude variations in flux over 100 s timescales, make it clear that we are observing a new and unprecedented astrophysical object (Figure 4).

The peak luminosity corresponds to the Eddington luminosity of a $\sim 10^{10} M_\odot$ black hole. It is highly unlikely that a moderate sized galaxy like the host of Sw 1644+57 could contain such a massive black hole – indeed, our SED fitting of the host galaxy implies its total stellar mass is less than this value (see SOM). Hence Sw 1644+57 is either accreting at a super-Eddington rate, or has its total energy modified by relativistic beaming (or both). A companion paper (1) considers the possibility that the source of this event is the tidal disruption of a star around the central black hole.

The discovery of a new class of extremely energetic γ -ray transient after many years of intensive monitoring of the γ -ray sky highlights the rarity of this phenomenon. Studies of

similar events in the future may lead to insight into the nature and fuelling of active galactic nuclei, or even provide electromagnetic smoking guns of black hole – black hole mergers, where the debris of the merger can result in a stellar disruption rate of $\sim 0.1 \text{ yr}^{-1}$ (25), raising the possibility that sensitive observations could uncover multiple events from a single galaxy. However, we note that Sw 1644+57 has emitted most of its radiation over the three weeks of its apparent existence relatively smoothly. It was only the presence of short, powerful bursts early on that alerted us to its presence, thus raising the possibility that other similar, but rather less variable, objects could easily be going undetected. Future sensitive and wide field X-ray observations of the sky offer the promise of finding more events like Sw 1644+57, as well as new classes of X-ray and γ -ray transients.

References and Notes

1. C. Kouveliotou, *et al.*, *Nature* **393**, 235 (1998).
2. F. Aharonian, *et al.*, *Science* **309**, 746 (2005).
3. I. Donnarumma, *et al.*, *ApJL* **691**, L13 (2009).
4. N. Gehrels, E. Ramirez-Ruiz, D. B. Fox, *Annual Review of Astronomy and Astrophysics* **47**, 567 (2009).
5. J. Hjorth, *et al.*, *Nature* **423**, 847 (2003).
6. S. E. Woosley, J. S. Bloom, *ARA&A* **44**, 507 (2006).
7. J. C. Cummings, *et al.*, *GCN* **11823** (2011).
8. T. Sakamoto, *et al.*, *GCN* **11842** (2011).
9. H. Krimm, S. Barthelmy, *GCN* **11891** (2011).

10. J. Bloom, *et al.*, A relativistic jetted outburst from a massive black hole fed by a tidally disrupted star (2011). Submitted.
11. G. Leloudas, *et al.*, *GCN* **11830** (2011).
12. S. D. Barthelmy, *et al.*, *GCN* **11824** (2011).
13. A. Levan, N. Tanvir, K. Wiersema, D. Perley, *GCN* **11833**, (2011).
14. C. Thoene, *et al.*, *GCN* **11834** (2011).
15. S. B. Cenko, *et al.*, *GCN* **11874** (2011).
16. D. Hoffman, *et al.*, *GCN* **11933** (2011).
17. P. Predehl, J. H. M. M. Schmitt, *A&A* **293**, 889 (1995).
18. A. Zauderer, E. Berger, D. A. Frail, A. Soderberg, *GCN* **11836**, 1 (2011).
19. A. Zauderer, *et al.*, *GCN* **11841** (2011).
20. A. Brunthaler, *et al.*, *GCN* **11911** (2011).
21. C. Kouveliotou, *et al.*, *ApJ* **608**, 872 (2004).
22. J. A. Nousek, *et al.*, *ApJ* **642**, 389 (2006).
23. Y. Ueda, M. Akiyama, K. Ohta, T. Miyaji, *ApJ* **598**, 886 (2003).
24. D. W. Just, *et al.*, *ApJ* **665**, 1004 (2007).
25. N. Stone, A. Loeb, *MNRAS* **412**, 75 (2011).
26. F. Pineau, *et al.*, *A&A* **527**, A126 (2011).

27. L. C. Ho, *ApJ* **699**, 626 (2009).
28. D. A. Kann, *et al.*, *ApJ* **720**, 1513 (2010).
29. P. A. Evans, *et al.*, *MNRAS* **397**, 1177 (2009).
30. S. Komossa, *et al.*, *ApJL* **603**, L17 (2004).
31. We gratefully acknowledge the efforts of the many observatories whose data is presented here. We particularly thank Daniele Malesani for assistance in the calibration of the optical photometry, Mike Irwin for assistance with the UKIRT data, Derek Fox for help with the PTF data, and Kevin Hurley and J. Xavier Prochaska for assistance in obtaining the Keck data. Full acknowledgements are given in the Supplementary online material.

¹Department of Physics, University of Warwick, Coventry, CV4 7AL, UK

²Department of Physics and Astronomy, University of Leicester, Leicester, LE1 7RH, UK

³Department of Astronomy, University of California, Berkeley, CA 94720-3411, USA

⁴Space Telescope Science Institute, 3700 San Martin Drive, Baltimore, MD 21218, USA

⁵Dark Cosmology Centre, Niels Bohr Institute, University of Copenhagen, 2100 Copenhagen, Denmark

⁶NASA Einstein Fellow

⁷Universities Space Research Association, NSSTC, 320 Sparkman Drive, Huntsville, AL 35805, USA

⁸Columbia Astrophysics Lab, Columbia University, NYC, NY 10024, USA

⁹Instituto de Astrofísica de Andalucía (IAA-CSIC), Glorieta de la Astronomía s/n, E-18008 Granada, Spain.

¹⁰Herschel Science Operations Centre, ESAC, ESA, PO Box 78, 28691 Villanueva de la Caada, Madrid, Spain

¹¹UCO/Lick Observatory, University of California, Santa Cruz, 1156 High Street, Santa Cruz, CA 95064, USA

¹²Institut de RadioAstronomie Millimétrique, 300 rue de la Piscine, Domaine Universitaire, 38406 Saint Martin d'Hères, France

¹³Joint Astronomy center, 660 North A'ohoku Place, University Park, Hilo, HI 96720, USA

- ¹⁴Center for Galaxy Evolution, University of California, Irvine, 4129 Frederick Reines Hall, Irvine, CA 92697
- ¹⁵Hubble Fellow
- ¹⁶ AIM, CEA/DSM - CNRS, Irfu/SAP, Centre de Saclay, Bat. 709, FR-91191 Gif-sur-Yvette Cedex, France
- ¹⁷Infrared Processing and Analysis Center, California Institute of Technology, Pasadena, CA, 91125, USA
- ¹⁶Centre for Astrophysics & Supercomputing, Swinburne University, Hawthorn VIC 3122, Australia
- ¹⁸Institute for the Physics and Mathematics of the Universe, University of Tokyo, Kashiwa-shi, Chiba 277-8568, Japan
- ¹⁹Cahill Center for Astrophysics, California Institute of Technology, Pasadena, CA, 91125, USA
- ²⁰Centre for Astrophysics & Cosmology, Science Institute, University of Iceland, Dunhaga 5, IS-107 Reykjavik, Iceland
- ²¹Center for Gravitation and Cosmology, University of Wisconsin-Milwaukee, 1900 E Kenwood Blvd, Milwaukee, WI - 53211, USA
- ²²Space Science Office, VP62, NASA/Marshall Space Flight Center Huntsville, AL 35812, USA
- ²³SLAC National Accelerator Center, Kavli Institute for Particle Astrophysics and Cosmology, 2575 Sand Hill Rd, MS 29, Menlo Park, Ca 94025, USA
- ²⁴Dunlap Institute for Astronomy & Astrophysics, University of Toronto, Toronto M5S 3H4, Ontario, Canada
- ²⁵Computational Cosmology Center, Lawrence Berkeley National Laboratory, 1 Cyclotron Road, Berkeley, CA 94720, USA
- ²⁶Astronomical Institute, University of Amsterdam, Science Park 904, 1098 XH Amsterdam, The Netherlands
- ²⁷Netherlands Institute for Radio Astronomy (ASTRON), Postbus 2, 7990 AA Dwingeloo, The Netherlands
- ²⁸Benoziyo Center for Astrophysics, Faculty of Physics, Weizmann Institute of Science, Rehovot, 76100, Israel
- ²⁹Department of Physics and Astronomy, Johns Hopkins University, Baltimore, MD 21218

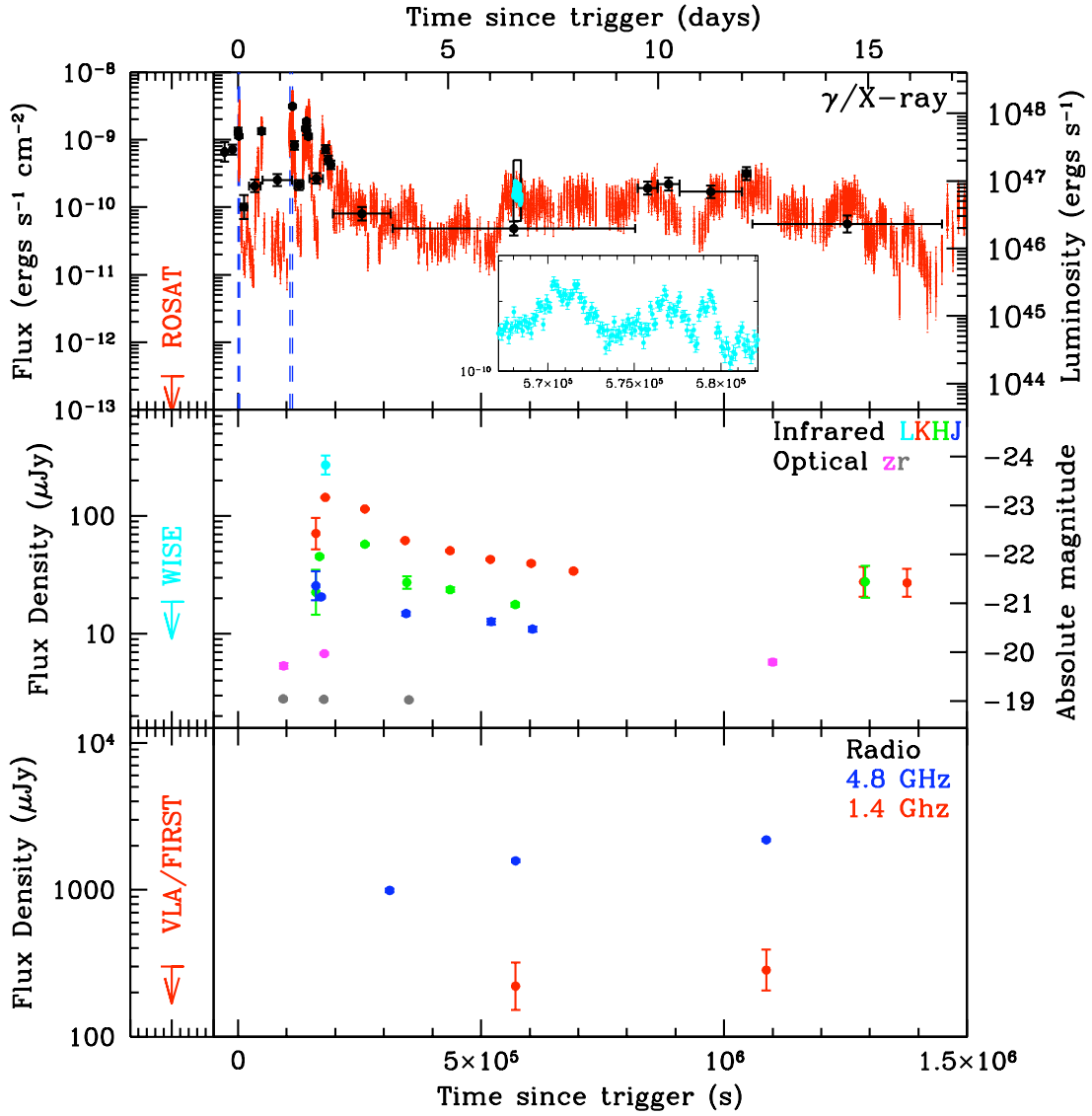


Figure 1: **The X-ray, infrared and radio lightcurves of Sw 1644+57:** The top panel shows the XRT (0.3–10 keV; in red) and BAT (15–50 keV; in black) flux against observed time since the initial outburst trigger time, where the right hand axis indicates the luminosity of the event. The inset panel shows the dense sampling of our *Chandra* observation. The dashed blue vertical lines show the times of subsequent triggers of the BAT. The middle-panel shows our nIR lightcurve of this event (host flux not subtracted). The lower panel shows our 4.8 GHz lightcurve obtained from the WSRT, demonstrating a rising radio lightcurve. The left hand panels represent pre-existing observation of the location of Sw 1644+57 and the limits on transient emission at this time (*I*), they clearly demonstrate the large amplitude of this outburst in the X-ray and infrared.

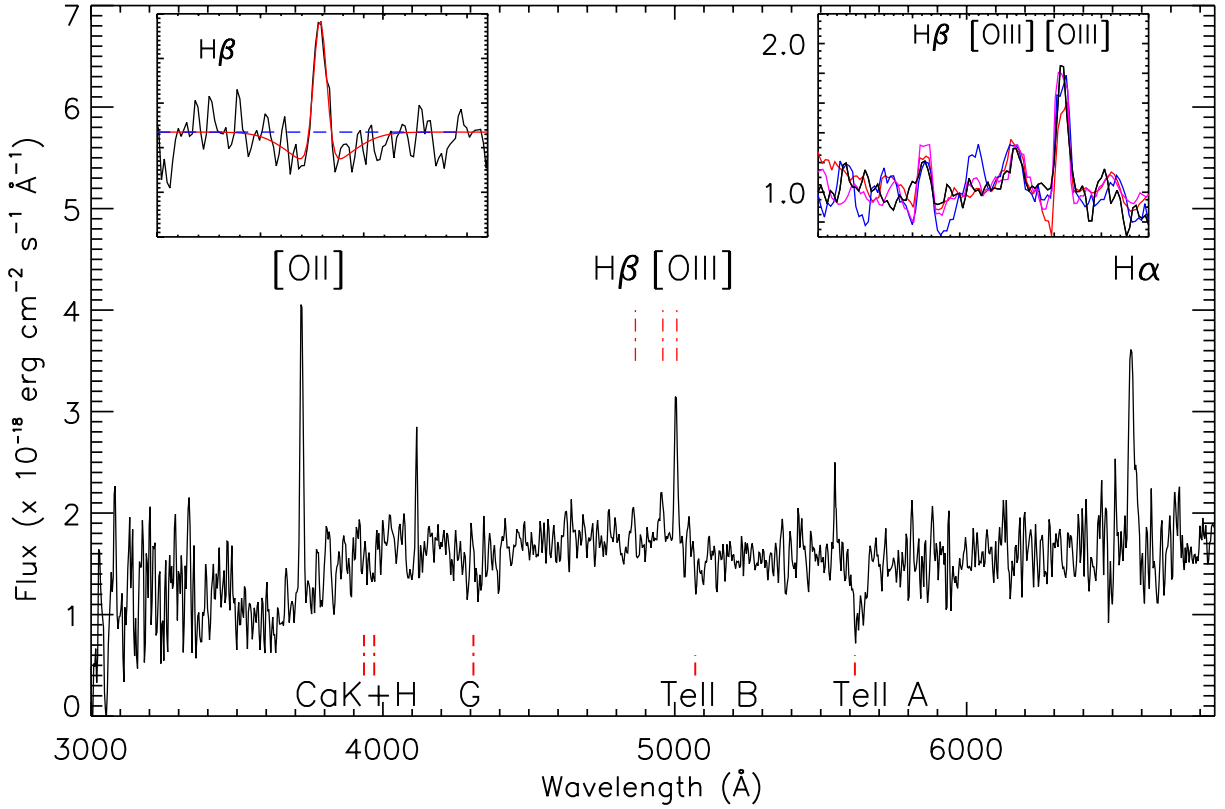


Figure 2: **Spectroscopy of the host galaxy of Sw 1644+57.** The main panel shows our observations obtained at the GTC plotted against rest-frame wavelength. The left inset shows the $H\beta$ line as seen in the first Gemini GMOS spectrum. Prominent stellar atmosphere absorption is visible. The inset on the right shows the first Gemini spectrum (red), the second Gemini spectrum (blue), the Keck spectrum (magenta) and the GTC spectrum (black) covering the $H\beta$ and [O III] doublet, all rebinned to the lower resolution of the GTC spectra. No emission line variability is apparent.

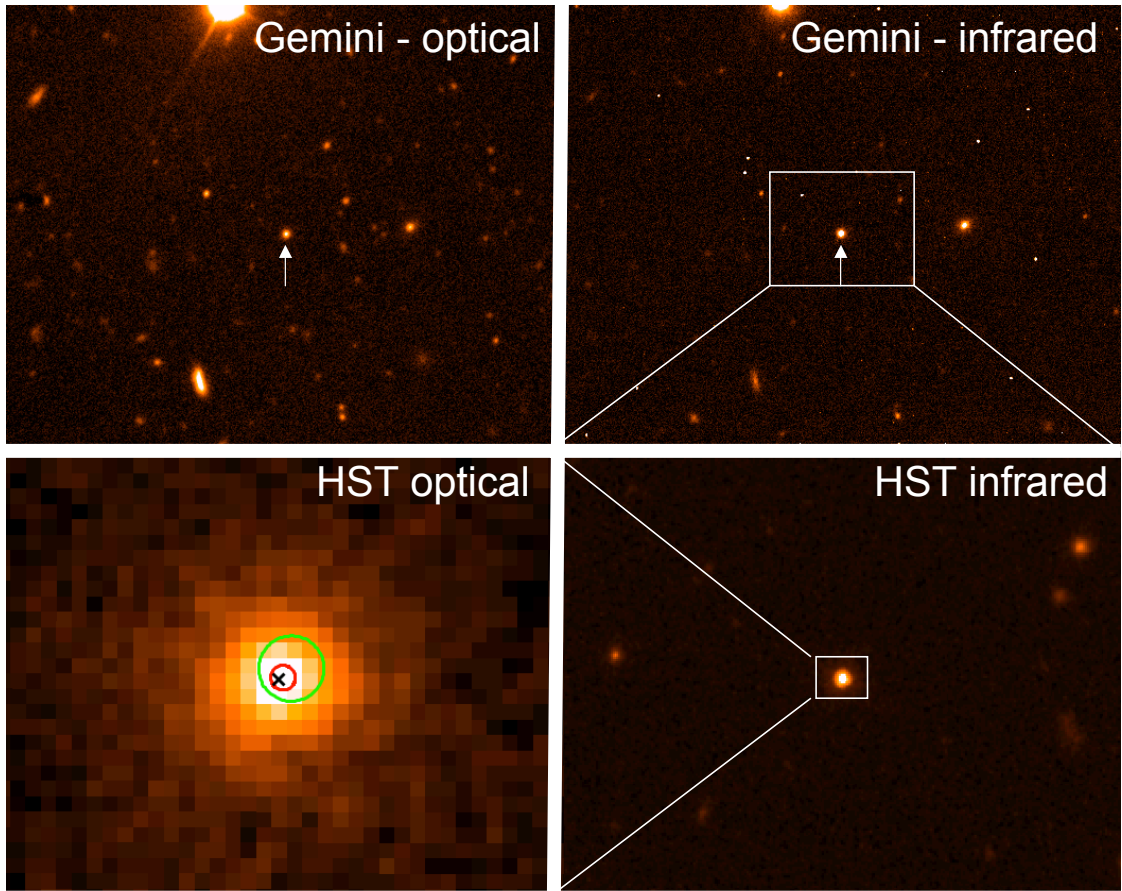


Figure 3: **Discovery images of Sw 1644+57 and its host galaxy.** The top panels show our ground based imaging in the optical r -band (top left), and infrared K -band (top right). The images are oriented north up, east left, and are approximately 1 arcminute in height, the location of Sw 1644+57 is indicated with arrows. The lower panels show zoomed in regions of our later time observations with *HST*. The source is unresolved in our WFC IR (F160W) imaging (bottom right), and is likely dominated by light from the transient. In contrast the source is clearly resolved in our WFC UVIS (F606W) imaging (bottom left, 1 arcsecond across), and contains at most a 30% contribution from the transient. This image also shows our astrometric constraints on the location of Sw 1644+57 upon its host. The cross hair indicates the optically derived centroid of the host galaxy. The blue circle shows the location of the transient inferred from our WFC IR observations, while the larger green circle shows the offset (due to the systematic uncertainty in tying coordinate frames) from our VLBI position. All available positions for the transient light are consistent with the center, and thus potentially the nucleus, of the galaxy.

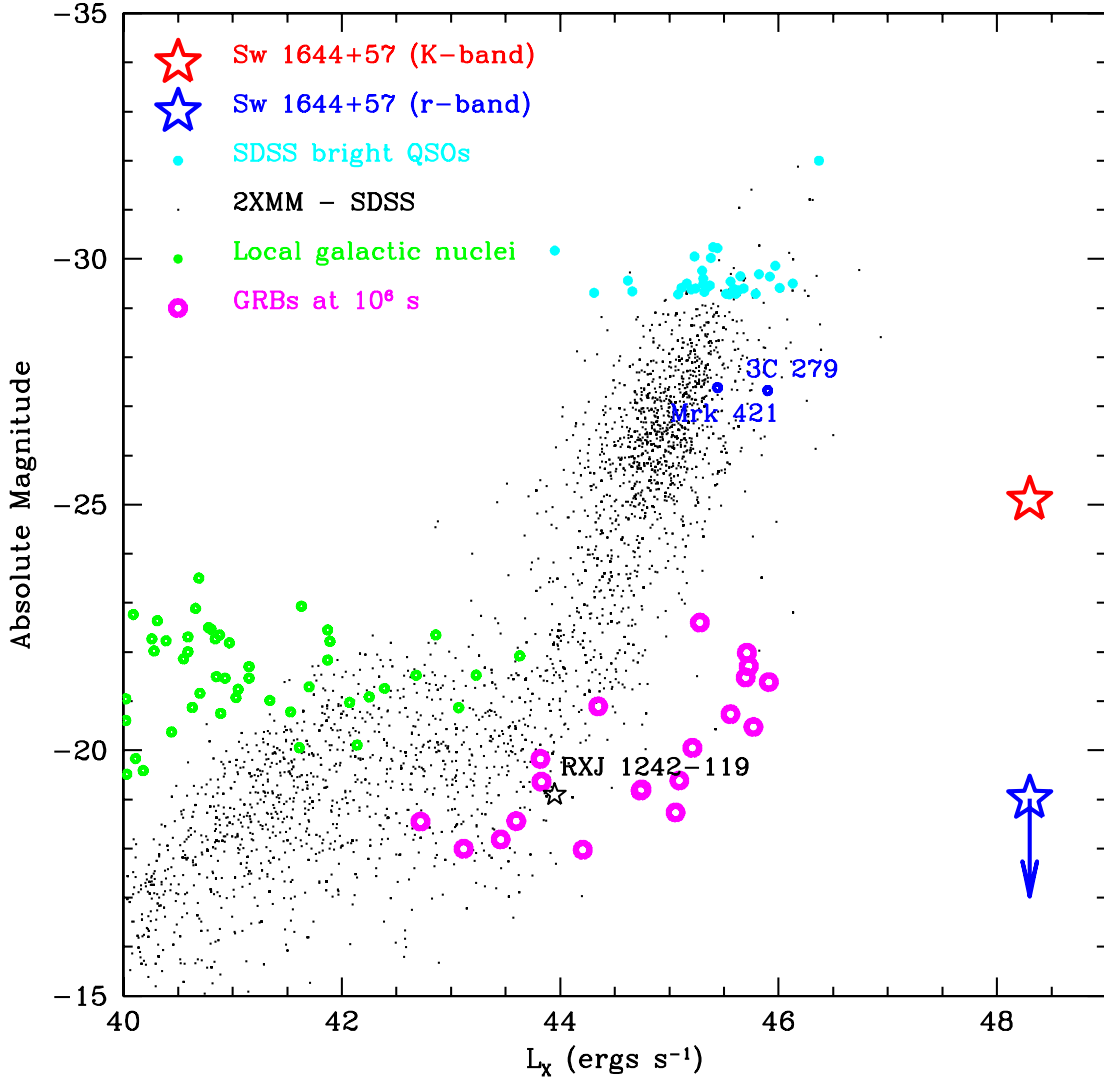


Figure 4: **The uniqueness of transient Sw 1644+57.** The plot shows the peak X-ray luminosity and optical/nIR absolute magnitude of Sw 1644+57, in comparison to the properties of the most luminous quasars and blazars (3C 279 and Mrk 421, marked). We show for comparison a sample of all objects within the 2XMM survey with high confidence ($> 2\sigma$) association with objects in SDSS of known redshift < 3 (based on (26)) and a sample of more local galaxies [from (27), note optical magnitudes include contribution from the host galaxy]. We also plot the late time luminosity of a sample of bright GRB afterglows (extrapolated from (15, 28)), which are relevant since Sw 1644+57 stays within an order of magnitude of its brightest peak, even 10^6 seconds after the outburst began. Finally, we also plot the location of the candidate tidal disruption event in RXJ 1242-119 (30), It is clear that in comparison with many other objects Sw 1644+57 is unique.

Supplemental Online Material:

“An extremely luminous panchromatic outburst from the nucleus of a distant galaxy”

We adopt cosmological parameters of $H_0 = 73 \text{ km s}^{-1} \text{ Mpc}^{-1}$, $\Omega_\Lambda = 0.73$ and $\Omega_m = 0.27$. At a redshift of $z = 0.3534$, the luminosity distance is 1814.8 Mpc and 1 arcsec represents 4.803 kpc in projection. These are identical parameters to those used in our companion paper (1)

1 The uniqueness of Sw 1644+57

In the main text we argue (in particular in Fig. 4) that Sw 1644+57 does not belong to any known class of high-energy transient sources, and therefore represents a novel astrophysical phenomenon. Here, we provide further justification of this claim by comparing Sw 1644+57 to other luminous optical, X- and γ -ray sources, in particular gamma-ray bursts (GRBs) and active galactic nuclei (AGN).

1.1 Comparison with gamma-ray bursts

A relatively wide variety of astrophysical sources are capable of generating sufficiently bright outbursts of high-energy radiation to trigger the current generation of gamma-ray satellites. These sources span an incredible range of the observable universe, from electrical discharges associated with thunderstorms on Earth (2) to the deaths of the earliest known stars (3, 4).

The association of Sw 1644+57 with a galaxy at $z = 0.3534$ immediately rules out all but the most luminous of these gamma-ray outbursts. While repeated high-energy triggers and rapid X-ray variability at late times have been seen before in events discovered by the *Swift* satellite¹, these sources are not known to generate anywhere near the total energy release observed from Sw 1644+57 ($E_{\text{iso}} \approx 10^{53}$ erg).

Gamma-ray bursts (GRBs) are the most luminous class of these high-energy transients ($L_{\text{iso}} \approx 10^{50}\text{--}10^{52} \text{ erg s}^{-1}$), and Sw 1644+57 was initially classified as a long-duration [i.e., resulting from massive star core-collapse (9)] GRB (10). But two important properties distinguish Sw 1644+57 from long-duration GRBs², clearly establishing it as a distinct class of high-energy transient.

First, unlike soft gamma-ray repeaters, long-duration GRBs are destructive events. The duration of the prompt gamma-ray emission, dictated by stellar debris accreting onto the newly-formed compact object, is typically $\Delta t \sim 1\text{--}10$ s. While late-time ($t \gg \Delta t$) engine activity can manifest as bright X-ray flares (11), no long-duration GRB has ever caused subsequent gamma-ray triggers of the *Swift* satellite in the manner of Sw 1644+57. The dramatically different timescale associated with the “prompt” emission (4 triggers over a period of 48 hours) is strongly suggestive of a distinct origin from long-duration GRBs.

In addition to the longer time scale associated with the gamma-rays, the X-ray (0.3–10 keV) emission from Sw 1644+57 is quite unlike any known GRB afterglow. In Figure 5 we compare the X-ray light curve of Sw 1644+57 with a representative sample of long-duration GRBs. While many GRBs exhibit an extended period of relatively flat emission [the so-called “plateau” phase (12)], no other long-duration GRB declines so little over the first ~ 2 weeks of its evolution. The long-lived light curve also makes the late-time emission significantly

¹For example, soft gamma-ray repeaters (5) can generate multiple high-energy triggers, and the unusual Galactic transient GRB 070610 exhibited dramatic X-ray and optical flaring not typically seen from gamma-ray bursts (6–8).

²Given the extreme duration and large luminosity, we also consider it extremely unlikely Sw 1644+57 is a member of the short-duration class of GRBs.

more luminous than normal long-duration GRBs. Together, the longer time scales associated with both the X-ray and gamma-ray emission, as well as the large X-ray luminosity, are indicative that a significantly more massive black hole is responsible for the observed emission from Sw 1644+57 [an idea explored in detail in our companion paper (1)].

Finally, we note that the astrometric coincidence with the center of the host galaxy is relatively unique amongst long-duration GRBs (at least those with observed with sufficiently high angular resolution). Given their association with star formation, it is not surprising that in general the location of long-duration GRBs is highly correlated with host galaxy light (in particular the blue light generated by massive stars (13, 14)). It is nonetheless unusual (though not unprecedented) for a long-duration GRB afterglow observed with the exquisite angular resolution of *HST* to be astrometrically consistent with the nucleus of its host galaxy.

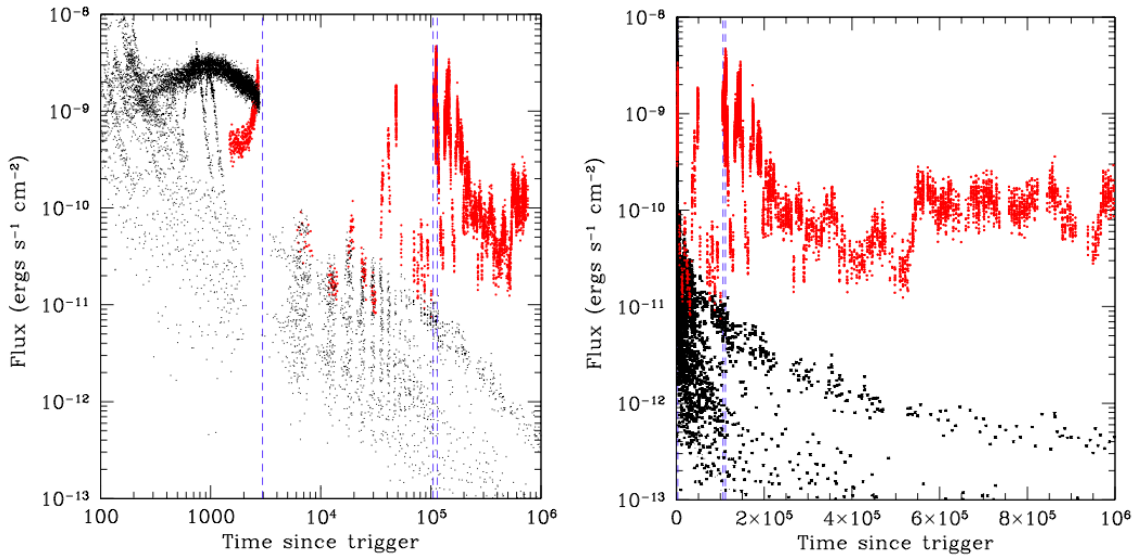


Figure 5: A comparison of the properties of Sw 1644+57 with those of GRB afterglows [from (15)]. The left hand panel shows a logarithmic time and flux axis, since GRBs usually decay as powerlaw's. The right hand panel shows the same plot, but with a linear time axis. It is clear that Sw 1644+57 is much longer lived than any GRB engine yet observed, and is two orders of magnitude brighter (in flux) at 10^6 s than observed for the brightest GRBs. No other GRB at similar redshift has ever appeared so bright at late times, and the afterglow of Sw 1644+57 is also a factor of 10-100 brighter in luminosity at late times than the brightest GRBs (see Figure 4, main article).

1.2 Comparison with active galactic nuclei

Given the long lived nature of the emission, and its location in the core of the host galaxy, it is also relevant to consider the comparison to the different manifestations of active galactic nuclei (AGN). The majority of AGN (e.g. LINERS, Seyferts, etc.) are of moderate X-ray and optical luminosity, and in this respect are not comparable to an exceptionally bright object like Sw 1644+57. The brighter AGN are the luminous quasars, and the blazars. These can reach X-ray luminosities approaching 10^{46} erg s^{-1} , with corresponding optical absolute magnitudes of

–30 or brighter. Furthermore, the blazars are intrinsically the most variable AGN, and can show rapid ~ 2 factor variation in their lightcurves. However, Sw 1644+57 exhibits much more rapid variability, of order a factor of 100 in just a few hundred seconds, and is also reaches peak luminosity in excess of 10^{48} ergs s^{-1} . This is shown graphically in Figure 4 of the main text where we compare the X-ray luminosity and optical absolute magnitude of Sw 1644+57 against those of QSO, Blazars, other AGN and GRB afterglows 10⁶ seconds post burst. As can be seen, Sw 1644+57 stands apart from any object previously observed, and leads us to conclude we are dealing with a previously unobserved, and extremely energetic phenomenon.

2 Observations

2.1 Pre-event imaging

2.1.1 Palomar Transient Factory (PTF)

As part of the Palomar Transient Factory [PTF (16, 17)], pre-outburst optical (R -band) imaging of the field of Sw 1644+57 were obtained with the Palomar 48 inch Oschin Schmidt telescope over the time period from 2009 May to 2010 October. In a stacked frame of all available data (77 individual images), we find a faint, unresolved source at location $\alpha = 16^{\text{h}}44^{\text{m}}49.983^{\text{s}}$, $\delta = +57^{\circ}34'59.72'$ (J2000.0). Astrometry was performed relative to 23 objects from the 2MASS point source catalog (18). The uncertainty in this position, including both the statistical error in the centroiding process and systematic error from the astrometric tie, is ≈ 250 mas in each coordinate. Using stars in the field calibrated via our LRIS imaging, we measure a magnitude of $R = 22.09 \pm 0.26$. This is marginally brighter than the value derived from our post-outburst imaging; however, given the somewhat different filters and the large uncertainty in this measurement, we do not consider this discrepancy particularly significant.

2.1.2 Wide-field Infrared Survey Explorer (WISE)

In addition to the optical imaging described above, the location of Sw 1644+57 was observed by the Wide-field Infrared Survey Satellite (WISE) (19) between 25 - 28 Jan 2010. Observations were obtained in each of the 3.4, 4.6, 12 and 22 micron bands (W1–4 respectively), with a total of 39 individual images per band included in each filter co-add. The resulting limits are shown in Table 1. These images suggest the host galaxy itself is not extremely red, and confirm that the vast majority of the flux in our mid-IR measurement (see below) is originating in the afterglow.

Table 1: Catalog of WISE observations

Band	Limit (mag)	Flux (μ Jy)
W1	> 18.0	> 19
W2	> 16.2	> 57
W3	> 12.8	> 240
W4	> 9.55	> 1270

2.2 Optical imaging

We obtained extensive optical imaging of Sw 1644+57 using the Gemini-North Telescope, the Nordic Optical Telescope (NOT), the Gran Telescopio CANARIAS (GTC) and the Keck I telescope. A log of optical observations

Start (MJD)	Mid-point (s, post burst)	Telescope	Filter	exptime (s)	Magnitude
55648.6466644	9207	Gemini-N	<i>r</i>	240	> 22.40
55649.6094537	92797	Gemini-N	<i>r</i>	5 × 120	22.78 ± 0.02
55649.5994062	99273	Gemini-N	<i>g</i>	5 × 120	23.66 ± 0.05
55649.6194815	93662	Gemini-N	<i>z</i>	5 × 120	22.08 ± 0.05
55650.5779583	176475	Gemini-N	<i>r</i>	5 × 120	22.79 ± 0.02
55650.5879664	177340	Gemini-N	<i>z</i>	5 × 120	21.82 ± 0.02
55652.6031910	351462	Gemini-N	<i>r</i>	5 × 120	22.80 ± 0.02
55649.1858626	57121	GTC	<i>i</i>	4 × 60	22.29 ± 0.05
55661.2350123	1100079	GTC	<i>z</i>	8 × 90	22.00 ± 0.05
55655.56435	607871	Keck	B	5 × 330	24.35 ± 0.05
55655.56480	607942	Keck	<i>i</i>	5 × 300	22.31 ± 0.02
55649.0744306	50036	NOT	<i>B</i>	2 × 600	24.40 ± 0.10
55649.1199514	50745	NOT	<i>V</i>	2 × 600	23.17 ± 0.05
55649.1361632	52146	NOT	<i>R</i>	2 × 600	22.55 ± 0.03
55650.2109861	145362	NOT	<i>R</i>	3 × 600	22.51 ± 0.04
55656.1730903	660436	NOT	<i>R</i>	3 × 600	22.40 ± 0.06
55661.0701887	1083334	NOT	<i>R</i>	4 × 300	22.44 ± 0.06

Table 2: Optical photometry of Sw 1644+57, obtained from Gemini-N, the GTC and the NOT.

is shown in Table 2. The data were all processed through IRAF in the normal way, and magnitudes and fluxes were extracted via aperture photometry of the source in comparison to objects in the field. Photometric calibration was based on standard stars, observed by the Nordic Optical Telescope, and confirmed by comparison to published zeropoints for our Gemini-North observations.

To search for variability we performed point spread function matched image subtraction, using the ISIS package (20). To obtain the cleanest subtractions we limit ourselves to images taken from the same telescope on different nights. Since each telescope offers a reasonable time baseline this enables us to search for optical variability over the course of the first week post burst.

In our optical (*r*- and *R*-band) imaging there is no evidence for any variable source within the host galaxy of Sw 1644+57, with the most constraining limits coming from our Gemini observations. To estimate the limiting magnitude of these subtractions we seed our first epoch images with artificial point spread functions of known magnitude, and use these to photometrically calibrate our subtracted images. From this we estimate that any variable source within the host of Sw 1644+57 had a magnitude fainter than $r > 25.5$ (3σ), in our earliest observations. This evidence does not necessarily preclude the presence of an optically variable transient which contributes similar flux to all epochs over our range of observation to date, however, it suggests that the variation in the flux between the observations was $< 0.23 \mu\text{Jy}$.

While our *r*-band observations do not yield any evidence of transient emission, we clearly detect a variable source in our *z*-band imaging, as shown in Figure 6. The source is seen to brighten between our first and second epoch of *z*-band observations which were taken 26 and 49 hours after the initial outburst. The X-ray lightcurve over the same time period is also seen to brighten, although by a much larger amplitude.

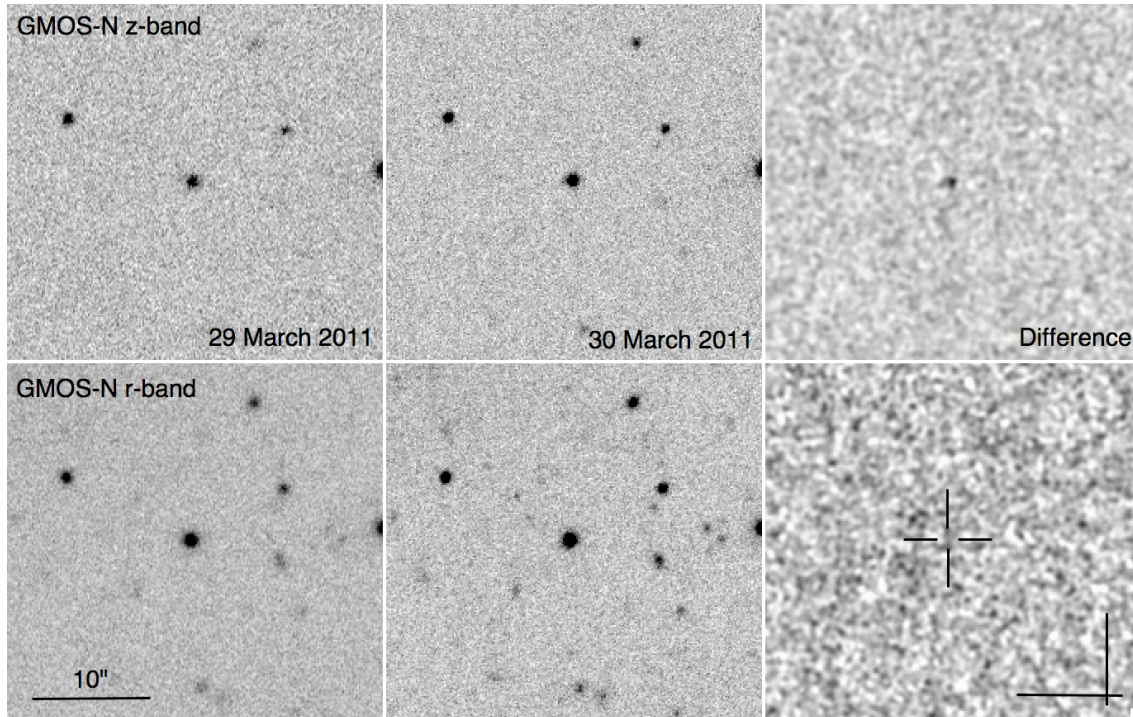


Figure 6: Our Gemini/GMOS imaging of Sw 1644+57. The top panels show of z -band imaging obtained on 29 and 30 March 2011, and the result of a PSF matched image subtraction. The bottom panels represent the same, but for our r -band imaging. In the z -band we clearly see residual emission, brightening between the two observations. In the r -band, no such variation is obvious, consistent with Sw 1644+57 originating on a highly dusty sightline which diminishes the transient optical flux. Images are North up and East to the left

2.3 Infrared imaging

We obtained IR observations of Sw 1644+57 with PAIRITEL, UKIRT and Gemini-North. A log of observations is shown in Table 3. The PAIRITEL and UKIRT observations were both pipeline processed using dedicated, instrument specific pipelines. The Gemini-North data were reduced using the standard NIRI package within IRAF. Photometric calibration was taken relative to 2MASS, and the resulting photometry is shown in Table 3.

We additionally obtained thermal IR observations of Sw 1644+57 with NIRI in the L -band. For this we used the 30 co-adds of 1 s exposures at each of 58 random dither positions, and used the f/32 camera to avoid saturation. Unfortunately in this imaging both the science and standard observations (of FS 138) showed substantial elongation of the point spread function. However, we were able to extract detection of the afterglow of Sw 1644+57. This provides a magnitude of $L' = 14.9 \pm 0.2$ (vegamag), or, correspondingly a flux of 0.27 ± 0.05 mJy at 3.78 microns.

2.4 Limits on rapid variability

We obtained 81, 20-second observations of Sw 1644+57 in the i -band with OSIRIS on the GTC on 30 March 2001. We can use these to place limits on any rapid variability within the optical data, similar to that observed in the X-rays. Photometry of the counterpart relative to two comparison stars in the image, shows no sign of variability

MJD start	Mid point	Mag	Telescope	Band
55649.35609	71588	> 19.1	PAIRITEL	J
55650.34888	161627	19.511 ± 0.284	PAIRITEL	J
55650.49898	170821	19.747 ± 0.023	UKIRT	J
55652.52602	345289	20.100 ± 0.040	UKIRT	J
55654.55962	520974	20.270 ± 0.057	UKIRT	J
55655.53639	605811	20.429 ± 0.049	UKIRT	J
55649.35609	71588	> 18.2	PAIRITEL	H
55650.34888	161627	19.068 ± 0.435	PAIRITEL	H
55650.45965	167400	18.311 ± 0.023	UKIRT	H
55651.55957	261049	18.050 ± 0.019	Gemini	H
55652.55021	347371	18.861 ± 0.023	UKIRT	H
55653.58889	436380	19.014 ± 0.044	Gemini	H
55655.13265	570064	19.330 ± 0.040	HST	H
55663.47546	1290643	18.846 ± 0.309	UKIRT	H
55649.35609	71588	> 16.9	PAIRITEL	K
55650.34888	161627	17.353 ± 0.306	PAIRITEL	K
55650.60548	178995	16.586 ± 0.007	Gemini	K
55651.55476	260634	16.833 ± 0.010	Gemini	K
55652.50449	343327	17.502 ± 0.015	UKIRT	K
55653.58405	435965	17.717 ± 0.019	Gemini	K
55654.53582	518918	17.903 ± 0.022	UKIRT	K
55655.50653	603003	17.988 ± 0.022	UKIRT	K
55656.51323	689990	18.149 ± 0.023	UKIRT	K
55663.41583	1287023	18.379 ± 0.294	UKIRT	K
55664.46310	1376628	18.401 ± 0.272	UKIRT	K

Table 3: Infrared photometry of Sw 1644+57

over the time baseline of the observations. Given the non-detection of any afterglow emission in the deep r-band images taken with Gemini-N the non-detection of rapid variability within these images is not surprising.

In addition, the short timescales for IR observations naturally lend themselves to studies of short time scale variation. We therefore photometer our individual NIRI frames separately, and find no evidence for rapid variability during their timeframe.

At first sight this would seem to imply that the IR variations, while tracking the broad shape of the X-ray lightcurve, do not show evidence for rapid variation. However, we note that at the time of our first epoch of NIRI observations (which provide 18x60s resolution) the X-ray afterglow of Sw 1644+57 was also not apparently rapidly variable.

2.5 Optical spectroscopy

We obtained multiple epochs of spectroscopy of Sw 1644+57 using the GTC, Gemini-North and Keck II telescopes. Data reduction and analysis of these data is provided below.

The first spectroscopy of Sw 1644+57 was obtained using the OSIRIS instrument on the 10.4m Gran Telescopio CANARIAS (GTC), starting 15.7 hours after the burst. We used the R300B grism with a 1 arcsecond wide slit and a 2×2 binning, taking three exposures of 1200 seconds starting on 04:43 UT on March 29, 2011. Data were reduced using tasks in IRAF, using calibration data (bias frames, flatfields and arc frames) taken the same night. Flux calibration was done using spectra of standard star Ross 640.

We obtained two epochs of spectroscopy of the transient and its host galaxy using the Gemini Multi-Object Spectrograph (GMOS) on Gemini-North. The first spectrum was taken using the R400 grating with a $1.0''$ slit width and using a standard 2×2 binning. Four 600 s exposures were taken, using dithers in spatial and dispersion directions (central wavelengths 6000 and 6050 Å), with observations starting at 13:16 UT on March 29, 2011.

The second spectrum was taken using the same grism, slitwidth and binning, but used a central wavelength of 8000 Å. Two exposures of 720 s were obtained in the so-called “nod & shuffle” mode to achieve accurate subtraction of nightsky emission lines (21). No dithering in dispersion direction was performed. Observations started 14:51 UT on April 1st, 2011.

The data of both epochs were reduced using the Gemini GMOS data reduction packages within IRAF. Flatfields and Cu+Ar arc lamp spectra taken just before the science data were used for calibration. Flux calibration was achieved using observations of standard star Hiltner 600 (22) and photometry was used to bring the spectra to an absolute flux scale. Finally, the spectra were corrected for a Galactic reddening of $E(B - V) = 0.02$, assuming $R_V = 3.1$.

Finally, we obtained moderate-resolution ($R \equiv \lambda/\Delta\lambda \approx 2500$) spectra at the location of Sw 1644+57 with the DEep Imaging Multi-Object Spectrograph [DEIMOS; (23)] mounted on the 10 m Keck II telescope on 2011 March 31 (beginning at 14:55 UT) and 2011 April 4 (beginning at 14:38 UT). The instrument was configured with the 600 lines mm^{-1} grating with a central wavelength of 6900 Å (7200 Å) on 2011 March 31 (2011 April 4), providing a spectral resolution of 3.5 Å (FWHM) and wavelength coverage from ≈ 4500 –9500 Å. We implement a modified version of the DEEP2 DEIMOS pipeline³ to rectify and background-subtract our spectra. The pipeline bias-corrects, flattens, traces the slit, and fits a two-dimensional wavelength solution to the slit by modeling the sky lines. This final step provides a wavelength for each pixel. The slit is then sky subtracted (in both dimensions) and rectified, producing a rectangular two-dimensional spectrum where each pixel in a given column has the same wavelength. From this point we proceed with standard reduction procedures, using the standard star BD+33 2642 for flux calibration. To account for slit losses, we renormalized each spectrum based on the observed R -band magnitude of the optical counterpart ($R = 22.6$ mag).

³See <http://astro.berkeley.edu/~cooper/deep/spec2d/>

Observed Wavelength Å	Line Flux (10^{-17} erg cm $^{-2}$ s $^{-1}$)	Identification	Redshift
5043.43 ± 0.53	3.5 ± 0.6	[OII]	0.35357
5047.41 ± 0.75	8.6 ± 1.4	[OII]	0.35362
6578.75 ± 0.42	2.7 ± 0.6	H β	0.35327
6711.26 ± 0.39	1.4 ± 0.4	[OIII]	0.35337
6775.85 ± 0.47	4.0 ± 0.5	[OIII]	0.35332
8881.45 ± 0.55	7.6 ± 1.0	H α	0.35329
8908.00 ± 0.83	1.2 ± 0.5	[NII]	0.3509
9089.11 ± 0.71	1.1 ± 0.3	[SII]	0.35326
9109.13 ± 0.69	0.9 ± 0.3	[SII]	0.35335

Table 4: Optical emission lines from Sw 1644+57 based on our Keck DEIMOS observations. These line fluxes are also consistent with those inferred from our GTC and Gemini observations.

2.6 Host spectroscopic properties

In our spectra we find nebular emission lines corresponding to [OII] $\lambda\lambda 3726, 3728$, H β , [OIII] $\lambda\lambda 4959, 5007$, H α , [NII] $\lambda 6583$, and [S II] $\lambda\lambda 6716, 6731$, all at a common redshift of $z = 0.3534 \pm 0.0002$, consistent with previously reported values (24, 25). A listing of all well-detected emission lines, with emission fluxes and centroids determined from Gaussian fits, is provided in Table 4, based on measurements from our Keck spectroscopy. The uncertainties in the line fluxes are dominated in nearly all cases by uncertainty in the strength of the continuum emission. All lines are unresolved, both spectrally and spatially, and show no significant evidence of variability between epochs (see Figure 2, main article).

We can estimate the extinction along the line of sight to the source using the observed intensity ratios of host-galaxy Balmer emission lines. We find that $(L_{H\alpha}/L_{H\beta})_{\text{obs}} = 2.8 \pm 0.6$. Assuming Case B recombination (26) and the relation from (27), we find $E(B - V)_{\text{gas}} = -0.01 \pm 0.15$ mag. Applying the extinction law derived for star-forming galaxies [e.g., (27)], this corresponds a limit on the rest-frame V -band extinction for the stellar continuum of $A_V < 0.8$ mag (3σ).

To determine the origin of these emission lines, we resort to a diagnostic, or BPT diagram [Baldwin, Phillips & Terlevich (28, 29)]. The atoms could be ionised by the hard power-law spectrum generated by gas accretion onto a central SMBH (i.e., an AGN), UV photons from young, massive O and B stars (i.e., star formation), or as part of a phenomenon known as a Low Ionisation Nuclear Emission-line Region [LINER; (30)], which are likely related to AGN, possibly resulting from changes to the geometry of the disc at low accretion levels (e.g., (31)). The observed ratios between various atomic species, since they are highly sensitive to the nature of the ionizing continuum, can be used to distinguish between these alternatives.

In figure 7, (SOM) we plot the ratio of $L_{[\text{O III}]\lambda 5009}/L_{H\beta}$ against $L_{[\text{N II}]\lambda 6583}/L_{H\alpha}$. Empirical (32, 33) and theoretical (34) dividing lines between the various classes of objects are plotted, as well as a series of analogous measurements from the MPA/JHU value-added SDSS catalog⁴. The optical counterpart of Sw 1644+57 clearly falls within the phase space of star-forming galaxies. In other words, there is no evidence for nuclear activity (i.e., an AGN) based solely on the optical spectra (35).

We can calculate the current star formation rate based on the strength of the H α and [O II] emission lines. Using the calibration from (36), we find $\text{SFR}_{H\alpha} = 0.3 \pm 0.1 M_{\odot} \text{ yr}^{-1}$, and $\text{SFR}_{[\text{O II}]} = 0.7 \pm 0.2 M_{\odot} \text{ yr}^{-1}$. Taking the average, we adopt a value of $\text{SFR} \approx 0.5 M_{\odot} \text{ yr}^{-1}$; the errors above likely underestimate the true uncertainty, as

⁴See <http://www.mpa-garching.mpg.de/SDSS>.

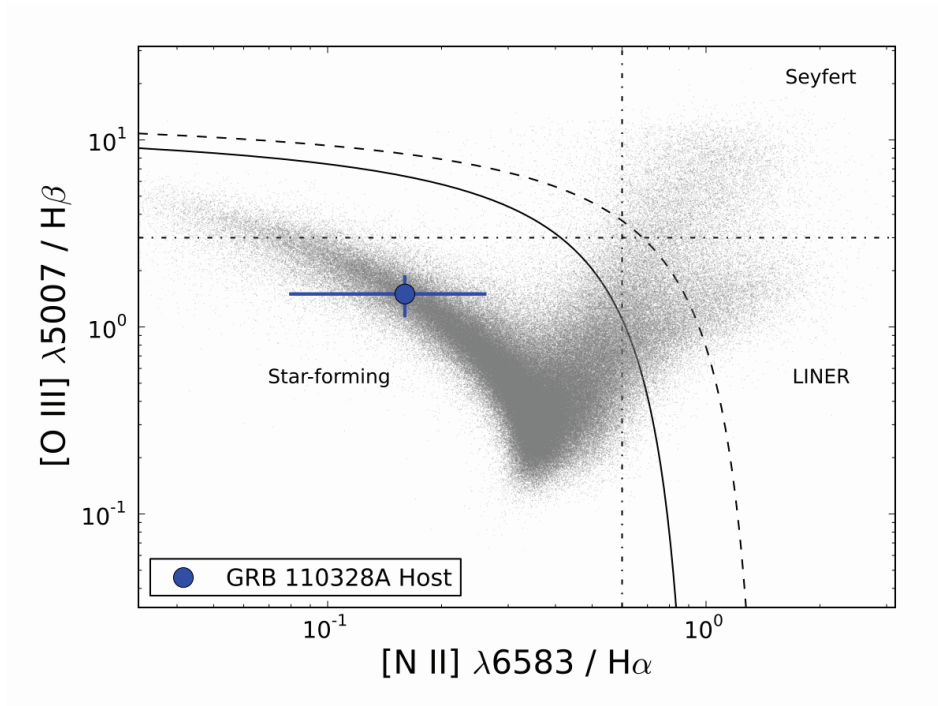


Figure 7: Diagnostic emission-line diagrams for the optical counterpart of Sw 1644+57. The empirical dividing line between star-forming and active galaxies from (32) is shown as the solid line, while analogous dividing lines from (33) are indicated with dashed-dotted lines. The theoretical dividing line from (34) is plotted as a dashed line. Analogous measurements for SDSS galaxies from the MPA-JHU value-added catalog are shown as gray dots. The optical counterpart falls firmly on the locus of star-forming galaxies, with no indication for any previous nuclear activity (i.e., an AGN).

they do not incorporate any effects of the assumed star-formation calibration.

Using the derived line fluxes from Table 4, we have measured the metallicity of the host galaxy based on our DEIMOS and GMOS spectra following the technique described in (37). Using the scales from (38) (PP04), we find $12 + \log(\text{O}/\text{H}) = 8.38 \pm 0.16$ based on the N 2 / H α diagnostic (PP04-N2H α), and $12 + \log(\text{O}/\text{H}) = 8.43^{+0.12}_{-0.14}$ based on the O 3 / N 2 (PP04-O3N2) prescription. Likewise, we find $12 + \log(\text{O}/\text{H}) = 8.60^{+0.19}_{-0.17}$ on the scale of (34) (KD02), and $\log(\text{O}/\text{H}) = 8.53 \pm 0.22$ on the scale of (39) (M91). Given the most recent estimate of the solar oxygen abundance [$\log(\text{O}/\text{H}) = 8.70$; (40)], together with the relative robustness of T_e -based metallicity scale (41), which the PP04-O3N2 scale is close to, we conclude the host metallicity is $Z \approx 0.5Z_\odot$. A comparison with SDSS samples of galaxies, as well as those of SN Ib/c and GRBs is shown in Figure 8 (SOM). This suggests that the host of Sw 1644+57 has a typical metallicity for its luminosity.

In addition to emission lines, continuum emission is detected over most of the spectral range, showing many (stellar) absorption features (e.g., G band, Na I, Mg I, Fe I, Ca H + K, Balmer line absorption) characteristic of an older (older than a few hundred Myr) population. To derive the H β emission line flux we fit simultaneously the continuum, the stellar absorption component and the emission line flux, where the lines are fit using Gaussians. In the first Gemini spectrum, which has highest signal to noise, we find a restframe equivalent width for the H β absorption of $8.2 \pm 1.1 \text{ \AA}$. A similar fit on H δ is not possible as the signal to noise is too low to reliably characterize the absorption component. A similar fit on H γ suffers from the presence of residuals from a nearby telluric emission line in the red absorption wing, but a $\sim 4\sigma$ detection of absorption was found with restframe equivalent width $11.7 \pm 2.4 \text{ \AA}$.

2.7 Host photometric properties

In principle we can use SED fitting to the observed host photometry to extract measurements of the luminosity of the host of Sw 1644+57 in various wavebands. Of particular importance is the stellar mass, which among the global properties of a galaxy is most closely linked to the size of its the central black hole.

The stellar mass of a galaxy is normally estimated using a measurement of the rest-frame K -band ($2 \mu\text{m}$) luminosity multiplied by a constant (of order unity in Solar units). Unfortunately, as long as the transient remains bright, a direct measurement of the infrared host flux is impossible. Fortunately, the transient contributes much less to the optical light: the resolved HST F606W observations constrain the contribution of the transient to at most 30% of the light in this filter (see below), and blueward of this band the contribution should be even less. Even in the NIR, the faintest measurement in each filter can be used to place a conservative upper limit on the host-galaxy flux; further constraints are provided by WISE pre-imaging of the field at $3.4 \mu\text{m}$. Hence we can fit template models using these values as hard upper limits to allowable IR flux.

In Figure 9, we plot the photometric constraints on the galaxy flux (that is, with the transient light removed) against different models of the stellar SED using the population-synthesis templates of (42). While a diverse set of different models (from young starbursts to evolved, quiescent populations) are nominally consistent with the observations, we can nevertheless bracket the possible range of K -band fluxes and back out a maximum and minimum luminosity. Using a stellar mass-to-light ratio of $M_*/L_K = 0.4$ in Solar units (following (43)) the range of stellar masses consistent with the data is approximately $10^9 - 10^{10} M_\odot$.

2.8 Hubble Space Telescope

We obtained *Hubble Space Telescope* (HST) observations of Sw 1644+57 on 4 April 2011, beginning at 03:03 UT. At this epoch we observed four dithered exposures in F110W in the IR channel of the Wide Field Camera 3, and 3 dithered exposures in the F606W within the UVIS channel. These observations were combined with `multidrizzle` to provide images with final pixel scales of 0.067 and 0.033'' respectively.

The HST images contain two stars that are common to both the 2MASS (18) and UCAC3 (44) catalogs (see table 5). Both of these catalogs have small astrometric errors ($\leq 0.07''$); we therefore averaged their astrometric positions to provide an astrometric reference for our HST images. While both of these stars are heavily saturated

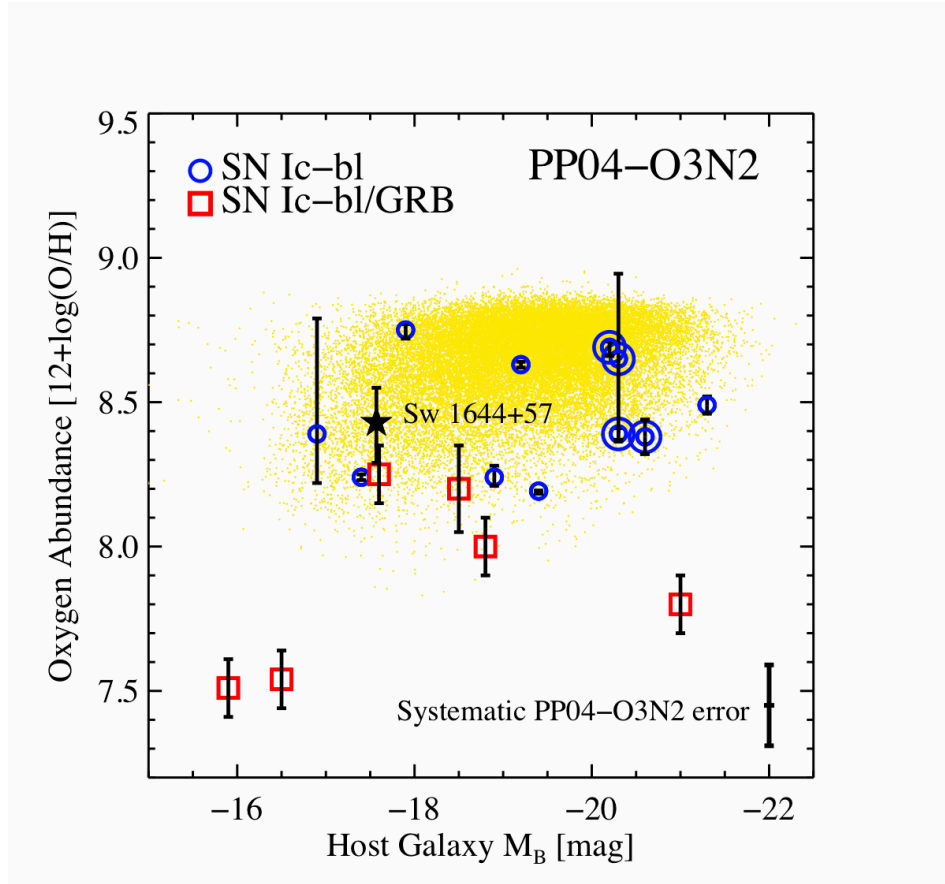


Figure 8: Host-galaxy luminosity (M_B) and host-galaxy metallicity (in terms of oxygen abundance) at the sites of Swift J164449.3+573451 (“Sw 1644+57”), nearby broad-lined SN Ic (SN Ic-bl: blue circles) and broad-lined SN Ic connected with GRBs (SN-bl/GRB): red squares). The oxygen abundances are in the (20) PP04-O3N2 scale. Yellow points are values for local star-forming galaxies in SDSS (25), re-calculated in the (20) scale for consistency, and illustrate the empirical luminosity-metallicity (LZ) relationship for galaxies. The host galaxy of Sw 1644+57 is broadly consistent with the bulk of SDSS galaxies at that luminosity. For more details see (37)

Star	ID	RA (J2000)	Dec (J2000)
A	2MASS 16445096+5735316	16:44:50.964	+57:35:31.64
B	2MASS 16444843+5734057	16:44:48.432	+57:34:05.74
A	3UC 296-121315	16:44:50.965	+57:35:31.69
B	3UC 296-121311	16:44:48.432	+57:34:05.82

Table 5: 2MASS and UCAC3 positions for two stars lying the field of view of our WFC3 UVIS and IR observations, and used for astrometric calibration. The ID’s A and B refer to the locations of the stars in Figure 10

in the WFC3/UVIS images, the saturation is mild in the WFC3/IR images. Thus centroiding the light will still give a position to an accuracy better than our drizzled pixel scale of 0.067 arcsec. Additionally it is possible to use the diffraction spikes of a bright star to estimate its location. These two methods agreed, again to a fraction of a drizzled IR pixel. As expected, the orientation and scale of the HST IR image World Coordinate System agreed within the errors with the astrometric positions of the two stars. We therefore used the stars only to update the absolute astrometric reference position of the image and not its orientation or scale. Following this procedure, we obtain a position for the IR source of RA = 16:44:49.9345, Dec = +57:34:59.673 J2000, with an estimated error of 0.07'' in each coordinate. Our derived position differs from the VLBA (see below) position by less than 0.03'' in both coordinates.

The host galaxy of GRB 110328A is clearly resolved in the *HST* WFC3 F606W image. The galaxy profile has a full-width half maximum (FWHM) of about 0.13'' compared to a FWHM of about 0.085'' for stars in the image. To determine a maximum contribution to the host galaxy magnitude from the transient we subtracted scaled stellar point source functions (PSFs) from both the centroid of the galaxy light, as well as from location of the IR source, which in our best estimate lies about 0.016'', from the galaxy centroid. We find that we subtract up to 20% of galaxy light in this manner without causing unreasonable deviations in the galaxy’s light profile. However, a PSF containing $\sim 30\%$ of the galaxy’s light causes clear errors, with depression of the central galaxy flux relative to the surroundings, and thus is a fairly hard upper limit to the total light in the transient. This corresponds to an F606W magnitude of 24.1 AB.

2.9 Chandra X-ray Observatory (CXO)

Following the discovery of the host galaxy of Sw 1644+57 we initiated Target of Opportunity observations with the *Chandra* X-ray Telescope. These observations were obtained on 4 April 2011, beginning at 02:30 UT, and utilised the High Resolution Camera in imaging mode (HRC-I). Using the standard cleaned event file we extract both images and lightcurves of the data, with the lightcurve shown in Figure 2 of the main paper, in 100s bins. The afterglow of Sw 1644+57 is strongly detected in the images, with a total of $\sim 50,000$ counts obtained over the course of the observation, at a mean count rate of ~ 3 counts per second. Since the HRC is primarily an imaging and timing instrument we do not create spectra, but instead convert counts to flux by assuming the spectral model from *Swift* XRT PC mode observations taken at approximately the same epoch.

We additionally perform astrometry between the CXO observations and our ground based Gemini and UKIRT observations. We identify 5 X-ray sources with optical counterparts in our UKIRT/Gemini image, and these are shown in Table 6. We then perform relative astrometry between these images, allowing us to place the position of the X-ray afterglow on the ground based frames with an accuracy of $\sim 0.25''$. The resulting position is offset $0.07 \pm 0.25''$ from the centre of the host galaxy, fully consistent with a nuclear origin.

Object	RA(J2000)	DEC(J2000)
Afterglow	16:44:49.905	57:34:59.82
1	16:45:05.036	57:37:41.41
2	16:44:22.354	57:35:43.88
3	16:44:21.893	57:36:15.17
4	16:44:41.285	57:35:04.94
5	16:45:02.019	57:37:40.99

Table 6: The locations of Chandra sources used for optical/X-ray astrometry. The positions are given in the world co-ordinate system of the Chandra image, but since relative astrometry is performed, the precise co-ordinates are not important.

2.10 Swift Observations

2.10.1 XRT

In Figure 1 (main article) we plot the X-ray lightcurve of Sw 1644+57 from the *Swift*-XRT and *Chandra*. This lightcurve was created following the method described in (15), and retrieved from the online XRT repository⁵. As noted in the main text the lightcurve is characterized by large scale variability, even at relatively late times after burst the variability is of order a factor 10^2 , on timescales of 1000 seconds. We highlight this in figure ?? (SOM), where we show zoomed in regions around two flares, which occurred on the second day. In particular we have overlaid these flares to a common time axis (by folding with a time period of 34300s) to demonstrate their broad similarity in morphology, especially during the decay.

In order to fit and describe the strong observed spectral variability (45, 46), we divide the XRT spectra into time-contiguous segments, containing > 500 cts (0.3–10 keV). This results in 139 PC mode spectra spanning the time 6.08 ksec to 1372.09 ksec after the BAT trigger and 461 WT mode spectra spanning the time 1.49 ksec to 191.67 ksec after the BAT trigger (with corresponding total exposures of 228.77 ksec and 14.33 ksec, respectively). The spectral reductions and fitting are performed as described in (47).

We find that the time-resolved spectra are well-fit by an absorbed powerlaw model with time-varying normalization, absorption column N_H , and photon index Γ . The average column in addition to the Galactic value ($1.66 \times 10^{20} \text{ cm}^{-2}$; (48)) is $(1.2 \pm 0.1) \times 10^{22}$ at $z = 0.35343$, and time variations about this value do not appear to be statistically significant. However, the flux and photon index exhibit a strong anti-correlation (see below). The time-average photon index is $\Gamma = 1.80 + / - 0.25$, dominated by the PC mode data with an average flux of $(1.6 \pm 0.9) \times 10^{-10} \text{ erg cm}^{-2} \text{ s}^{-1}$. (The quoted flux uncertainty here reflects the flux variation rather than the statistical uncertainty in any given 500 count epoch.) The WT mode data span a higher flux region of the emission ($(2.3 \pm 1.4) \times 10^{-9} \text{ erg cm}^{-2} \text{ s}^{-1}$) and have a harder mean photon index of $\Gamma = 1.6 \pm 0.2$, which is consistent with that measured for the BAT at similar epochs (see below). We note that the BAT lightcurve closely tracks the X-ray lightcurve.

As discussed in Kennea et al. (46) and Bloom et al. (45), the X-ray hardness tracks the X-ray flux. Consistently, we see that the best-fit powerlaw index increases with decreasing flux, with high-flux values corresponding to the quoted value of 1.6 for the WT mode data above and low-flux values just after the bright WT mode X-ray flares of $\Gamma = 3$. The spectra in these regions of flux decline can also be well-modelled assuming a (nearly) constant X-ray flux normalization and a fixed, single powerlaw index (e.g., $\Gamma = 1.6$), but allowing for an exponential cutoff which starts above the X-ray bandpass and passes into the X-ray bandpass as the source flux declines, reaching $E_{\text{cut}} \approx 1$ keV. The specific values for these cutoffs depends on the value we fix for Γ .

⁵http://www.swift.ac.uk/xrt_curves

2.10.2 BAT

In Figure 1 (main article) we also plot the BAT data. These data are taken from the online repository⁶ and were subsequently re-binned to have $S/N = 3$ (15-50 keV band). To convert these count rates to fluxes, we jointly fit the overlapping XRT data during the flare region from 2342.8 to 2715.1 ksec. Consistent with BAT only fits from (49) and the XRT-only fits described above, we find the BAT and XRT spectra are jointly described-well ($\chi^2/\nu = 587.0253/457$) by an absorbed powerlaw spectrum with photon index $\Gamma = 1.62 \pm 0.05$. The normalization at 1 keV is $0.48 \pm 0.03 \pm 0.5$ mJy, and the inferred column density is $N_H = 1.50 \pm 0.08 \times 10^{22}$ cm⁻² ($z = 0.3434$).

There is modest evidence ($3.2 - \sigma$ significant; $\Delta\chi^2 = 9.93$ for 1 additional degree of freedom) for a cutoff in the BAT spectrum at $\nu F\nu$ peak energy of $E_p = 71_{-22}^{+66}$ keV. Using this spectral fit, we convert the measured BAT count rate to 15-50 keV fluxes, which are overplotted on in Figure 1 of the main journal. This fit does not therefore take into account the fine detail that may be present in the spectral evolution over time, but shows broadly that the BAT flux does trace that seen with the XRT.

2.10.3 UVOT

The *Swift*-UVOT instrument began observing the field of Sw 1644+57 1482 s after the initial BAT trigger, starting the usual automatic sequence of observations. No optical or ultraviolet counterpart was detected at the location of Sw 1644+57 in either single frames or coadded images (50).

After the first two days, observations were obtained in “filter of the day” mode. We coadded these late-time observations using the `HEASOFT v6.10` distribution of the UVOT reduction tools. In particular a single combined frame has been obtained using the `uvotimsum` task. Upper limits were then obtained with the `uvotsource` task, following the procedure described by (51) and applying the latest UV filters zero points (52). In Table 7 we report 3σ limits for the bluest UVOT filters.

Time (UT)	Exposure (s)	Filter	Frequency (Hz)	Mag	Flux (mJy)
March 31	11220	<i>white</i>	8.64×10^{14}	> 23.94	$< 5.13 \times 10^{-4}$
March 31	11411	<i>u</i>	8.56×10^{14}	> 23.00	$< 9.05 \times 10^{-4}$
April 1	20899	<i>uvw1</i>	1.16×10^{15}	> 23.27	$< 4.37 \times 10^{-4}$
April 3	15235	<i>uvm2</i>	1.35×10^{15}	> 23.05	$< 4.65 \times 10^{-4}$
April 6	13030	<i>uvw2</i>	1.48×10^{15}	> 23.26	$< 3.66 \times 10^{-4}$

Table 7: Log of *Swift* UVOT observations and upper limits

2.11 VLBA Observations

Sw 1644+57 was observed on 1 and 3 April 2011 with the Very Long Baseline Array (VLBA). On both dates, observations began at 0530 UT and continued for 4 hours. Observations were obtained at a sky frequency of 8.4 GHz and with a recording bandwidth of 512 Mbps and correlated in full Stokes mode. The bright, compact source 3C 345 was used to calibrate instrumental delay and phase terms. The ICRS reference source J1638+5720 was used as phase calibrator in a switching cycle of 4 minutes with Sw 1644+57. Observations were also obtained of the nearby compact object J1657+5705 every 30 minutes. A prior amplitude corrections were applied. Calibration of the linear polarization leakage terms was obtained using J1638+5720. Each source was imaged in Stokes I, Q,

⁶<http://swift.gsfc.nasa.gov/docs/swift/results/transients/>

and U on both days. We also merged together visibility data from both dates and produced joint images. We show an image of the source in Stokes I and in polarized intensity in Fig. 12.

In Table 8 we summarize the results for GRB 110328A. We include results for each date and for the merged data. Columns give (1) the epoch of observation; (2) synthesized beam size; (3) seconds of right ascension; (4) arcseconds of declination; (5) flux density; (6) polarization fraction (2σ upper limit); and (7) rms fractional variations on hourly timescales (2σ upper limit). The coordinates are given relative to the position of ($16^h44^m, +57^\circ34'$).

The source is point-like in all three images, implying an upper limit to the size of ~ 1 mas. The compact source size confirms the non-thermal nature of the source and can be used to argue for relativistic motion (J). The source is constant in flux density between the two epochs and there is no evidence for variability on shorter timescales at a level of 17%. No linear polarization is detected with a 2σ upper limit of 2.7% in the merged data.

The positions are relative to the ICRS position of J1638+5720, $16^h38^m13.^s4563\ 57^\circ20'23.''979$. Formally, the position of the source changes by 177 ± 45 microarcsec and 73 ± 47 microarcsec between the two epochs. These differences are likely dominated by systematic errors, thus we do not believe the data require significant proper motion. Refined analysis including use of updated Earth orientation parameters may permit us to reduce systematic errors, and several further epochs are planned over the coming months. For reference note that an apparent motion of $10c$ will produce an offset of 174 microarcsec in 100 days.

2.12 Westerbork Synthesis Radio Telescope

We additionally obtained observations with the Westerbork Synthesis Radio Telescope (WSRT) at 1.4 and 4.8 GHz. We used the Multi Frequency Front Ends (53) in combination with the IVC+DZB back end in continuum mode, with a bandwidth of 8x20 MHz. Gain and phase calibrations were performed with the calibrators 3C 48 and 3C 286. The observations have been analysed using the Multichannel Image Reconstruction Image Analysis and Display (MIRIAD) (54) software package. We observed the source at three epochs, the first observation was carried out at 4.8 GHz, and the other two at both 1.4 and 4.8 GHz. A log of these observations and the resulting fluxes are shown in Table 9.

2.13 IRAM

The IRAM Plateau de Bure Interferometer [PdBI, France (55)] observed the Sw 1644+57 source on 31 March (22:10 UT - 1 Apr 00:35 UT) at 102.5 GHz, using its compact 5-antenna configuration. The counterpart was detected on the phase centre co-ordinates within the 3.36×2.30 arcsec (98.44 deg) primary beam of the antennas. The flux density measurement yielded 20.8 ± 0.1 mJy.

Acknowledgements

A.J.L. and N.R.T. acknowledge support from STFC. Swift, launched in November 2004, is a NASA mission in partnership with the Italian Space Agency and the UK Space Agency. Swift is managed by NASA Goddard. Penn State University controls science and flight operations from the Mission Operations Center in University Park, Pennsylvania. Los Alamos National Laboratory provides gamma-ray imaging analysis. S.B.C. acknowledges generous support from Gary and Cynthia Bengier, the Richard and Rhoda Goldman Fund, NASA/Swift grant NNX10AI21G, NASA/Fermi grant NNX10A057G, and NSF grant AST-0908886. A.J.vdH. was supported by NASA grant NNH07ZDA001-GLAST. GL is supported by a grant from the Carlsberg foundation. M.M. is supported by the Hubble Fellowship grant HST-HF-51277.01-A, awarded by STScI, which is operated by AURA under NASA contract NAS5-26555. The Dark Cosmology Centre is funded by the DNRF. This work makes use of data obtained by the Chandra X-ray Observatory (OBSID = 12920). Based on observations made with

the NASA/ESA Hubble Space Telescope (program ID 12447), obtained from the data archive at the Space Telescope Institute. STScI is operated by the association of Universities for Research in Astronomy, Inc. under the NASA contract NAS 5-26555. Based on observations obtained at the Gemini Observatory, which is operated by the Association of Universities for Research in Astronomy, Inc., under a cooperative agreement with the NSF on behalf of the Gemini partnership: the National Science Foundation (United States), the Science and Technology Facilities Council (United Kingdom), the National Research Council (Canada), CONICYT (Chile), the Australian Research Council (Australia), Ministério da Ciência e Tecnologia (Brazil) and Ministerio de Ciencia, Tecnología e Innovación Productiva (Argentina). The United Kingdom Infrared Telescope is operated by the Joint Astronomy Centre on behalf of the Science and Technology Facilities Council of the U.K. UKIRT data were processed by the Cambridge Astronomical Survey Unit. Based on observations made with the Nordic Optical Telescope, operated on the island of La Palma jointly by Denmark, Finland, Iceland, Norway, and Sweden, in the Spanish Observatorio del Roque de los Muchachos of the Instituto de Astrofísica de Canarias. Based on observations obtained with the Samuel Oschin Telescope at the Palomar Observatory as part of the Palomar Transient Factory project. The National Energy Research Scientific Computing Center, which is supported by the Office of Science of the U.S. Department of Energy under Contract No. DE-AC02-05CH11231, provided staff, computational resources and data storage for this project. The WSRT is operated by ASTRON (Netherlands Institute for Radio Astronomy) with support from the Netherlands foundation for Scientific Research. Some of the data presented herein were obtained at the W.M. Keck Observatory, which is operated as a scientific partnership among the California Institute of Technology, the University of California and the National Aeronautics and Space Administration. The Observatory was made possible by the generous financial support of the W.M. Keck Foundation. We acknowledge support by the Spanish Ministry of Science and Innovation (MICINN) under the project grant AYA 14000-C03-01 (including Feder funds) The NOT and the Gran Telescopio Canarias (GTC) are installed in the Spanish Observatorio del Roque de los Muchachos of the Instituto de Astrofísica de Canarias in the island of La Palma.

References and Notes

1. J. Bloom, *et al.*, Relativistic jetted emission powered by the tidal disruption of a star (2011). Submitted.
2. G. J. Fishman, *et al.*, *Science* **264**, 1313 (1994).
3. N. R. Tanvir, *et al.*, *Nature* **461**, 1254 (2009).
4. R. Salvaterra, *et al.*, *Nature* **461**, 1258 (2009).
5. P. M. Woods, C. Thompson, *In: Compact stellar X-ray sources. Edited by Walter Lewin & Michiel van der Klis. Cambridge Astrophysics Series* p. 547 (2006).
6. M. M. Kasliwal, *et al.*, *ApJ* **678**, 1127 (2008).
7. A. Stefanescu, *et al.*, *Nature* **455**, 503 (2008).
8. A. J. Castro-Tirado, *et al.*, *Nature* **455**, 506 (2008).
9. S. E. Woosley, J. S. Bloom, *ARA&A* **44**, 507 (2006).
10. J. C. Cummings, *et al.*, *GCN* **11823**, 1 (2011).
11. D. N. Burrows, *et al.*, *Science* **309**, 1833 (2005).
12. J. A. Nousek, *et al.*, *ApJ* **642**, 389 (2006).
13. J. S. Bloom, S. R. Kulkarni, S. G. Djorgovski, *AJ* **123**, 1111 (2002).
14. A. S. Fruchter, *et al.*, *Nature* **441**, 463 (2006).
15. P. A. Evans, *et al.*, *MNRAS* **397**, 1177 (2009).

16. N. M. Law, *et al.*, *PASP* **121**, 1395 (2009).
17. A. Rau, *et al.*, *PASP* **121**, 1334 (2009).
18. M. F. Skrutskie, *et al.*, *AJ* **131**, 1163 (2006).
19. E. L. Wright, *et al.*, *AJ* **140**, 1868 (2010).
20. C. Alard, *AAPS* **144**, 363 (2000).
21. K. Glazebrook, J. Bland-Hawthorn, *PASP* **113**, 197 (2001).
22. M. Hamuy, *et al.*, *PASP* **104**, 533 (1992).
23. S. M. Faber, *et al.*, *Society of Photo-Optical Instrumentation Engineers (SPIE) Conference Series*, M. Iye & A. F. M. Moorwood, ed. (2003), vol. 4841 of *Society of Photo-Optical Instrumentation Engineers (SPIE) Conference Series*, pp. 1657–1669.
24. A. J. Levan, *et al.* (2011). GCN Circular 11833.
25. C. C. Thone, *et al.* (2011). GCN Circular 11834.
26. D. E. Osterbrock, *Astrophysics of gaseous nebulae and active galactic nuclei* (1989).
27. D. Calzetti, *PASP* **113**, 1449 (2001).
28. J. A. Baldwin, M. M. Phillips, R. Terlevich, *PASP* **93**, 5 (1981).
29. S. Veilleux, D. E. Osterbrock, *ApJS* **63**, 295 (1987).
30. T. M. Heckman, *A&A* **87**, 152 (1980).
31. L. C. Ho, *ARA&A* **46**, 475 (2008).
32. G. Kauffmann, *et al.*, *MNRAS* **346**, 1055 (2003).
33. L. C. Ho, A. V. Filippenko, W. L. W. Sargent, *ApJS* **112**, 315 (1997).
34. L. J. Kewley, M. A. Dopita, *ApJS* **142**, 35 (2002).
35. S. B. Cenko, *et al.* (2011). GCN Circular 11874.
36. R. C. Kennicutt, *ARA&A* **36**, 189 (1998).
37. M. Modjaz, *et al.*, *AJ* **135**, 1136 (2008).
38. M. Pettini, B. E. J. Pagel, *MNRAS* **348**, L59 (2004).
39. S. S. McGaugh, *ApJ* **380**, 140 (1991).
40. M. Asplund, N. Grevesse, A. J. Sauval, P. Scott, *ARA&A* **47**, 481 (2009).
41. F. Bresolin, *et al.*, *ApJ* **700**, 309 (2009).
42. G. Bruzual, S. Charlot, *MNRAS* **344**, 1000 (2003).
43. J. M. Castro Cerón, *et al.*, *ApJ* **721**, 1919 (2010).
44. N. Zacharias, *et al.*, *VizieR Online Data Catalog* **1315**, 0 (2009).
45. J. Bloom, *et al.* (2011). GCN Circular 11847.
46. J. Kennea, *et al.* (2011). Astronomers Telegrams 3242.
47. N. R. Butler, D. Kocevski, *ApJ* **663**, 407 (2007).

48. P. M. W. Kalberla, *et al.*, *A&A* **440**, 775 (2005).
49. T. Sakamoto, *et al.*, *GCN* **11842** (2011).
50. A. A. . Breeveld, *et al.* (2011). GCN Circular 11910.
51. T. S. Poole, *et al.*, *MNRAS* **383**, 627 (2008).
52. A. A. Breeveld, *et al.*, *ArXiv e-prints* (2011).
53. G. H. Tan, *IAU Colloq. 131*, R. A. Shaw, H. E. Payne, & J. J. E. Hayes, ed. (1991), vol. 19 of *Astronomical Society of the Pacific Conference Series*, pp. 42–46.
54. R. J. Sault, P. J. Teuben, M. C. H. Wright, *Astronomical Data Analysis Software and Systems IV*, R. A. Shaw, H. E. Payne, & J. J. E. Hayes, ed. (1995), vol. 77 of *Astronomical Society of the Pacific Conference Series*, pp. 433–+.
55. S. Guilloreau, *et al.*, *A&A* **262**, 624 (1992).

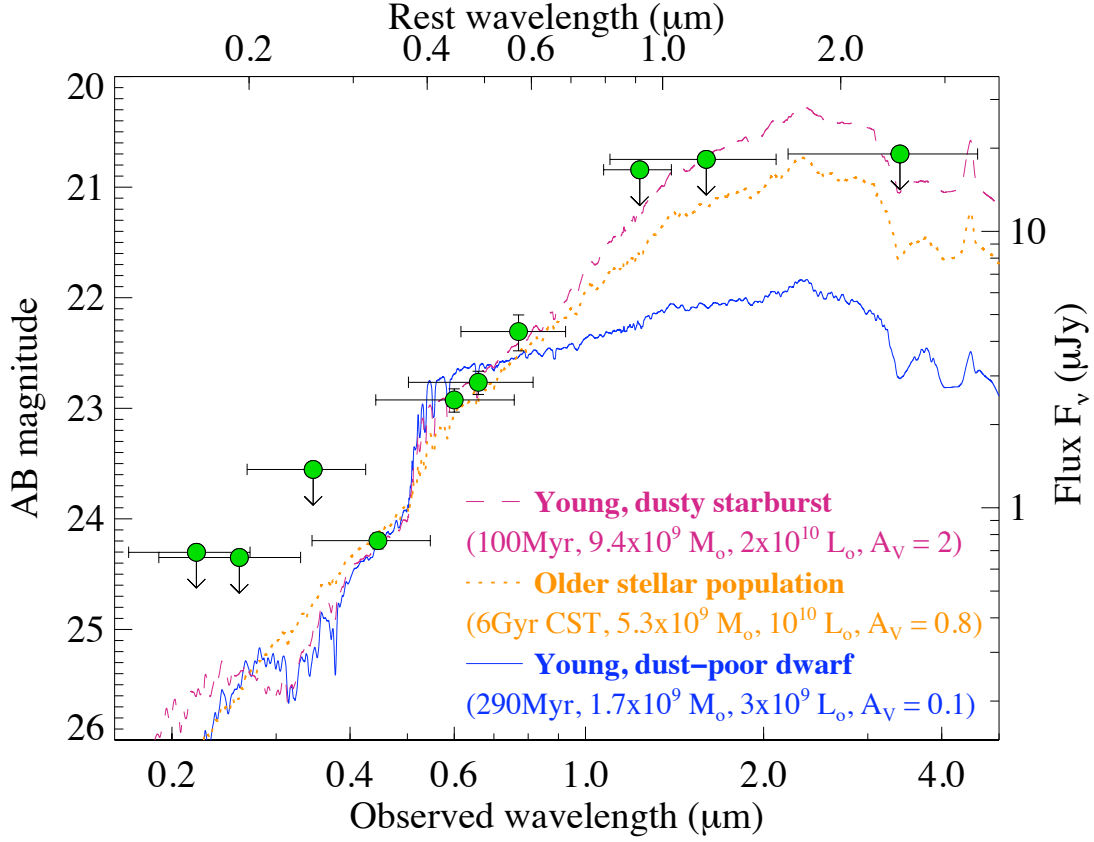


Figure 9: Photometry of the host galaxy of Sw 1644+57, matched to a variety of population-synthesis templates [BC2003] bracketing the range of possible IR colors. Optical/UV upper limits are provided by the UVOT, with the optical NIR points coming from our ground-based imaging and HST. The upper limit at $3.4 \mu\text{m}$ is from pre-imaging from WISE. Three population-synthesis bracketing the variety of possibilities are shown. Population ages (a single stellar population is assumed for the young models; continuous star formation is assumed for the older model), inferred stellar masses, bolometric luminosities, and total extinction for each model are indicated. (For clarity, the templates have been smoothed to a resolution of $\lambda/\Delta\lambda = 100$.)

Table 8: VLBA Results for GRB 110328A

Date	Beam (arcsec \times arcsec)	α (sec)	δ (arcsec)	S (mJy)	p	m
1 April 2011	$2.85 \times 1.76, 48^\circ$	$49.9313356 \pm 0.000004360$	59.689571 ± 0.00003562	1.7 ± 0.1	$< 4.5\%$	$< 34\%$
3 April 2011	$2.37 \times 1.00, 45^\circ$	$49.9313136 \pm 0.000003396$	59.689498 ± 0.00003083	1.7 ± 0.1	$< 4.7\%$	$< 34\%$
Average	$2.57 \times 1.24, 45^\circ$	$49.9313218 \pm 0.000002646$	59.689530 ± 0.00002331	1.68 ± 0.070	$< 2.7\%$...

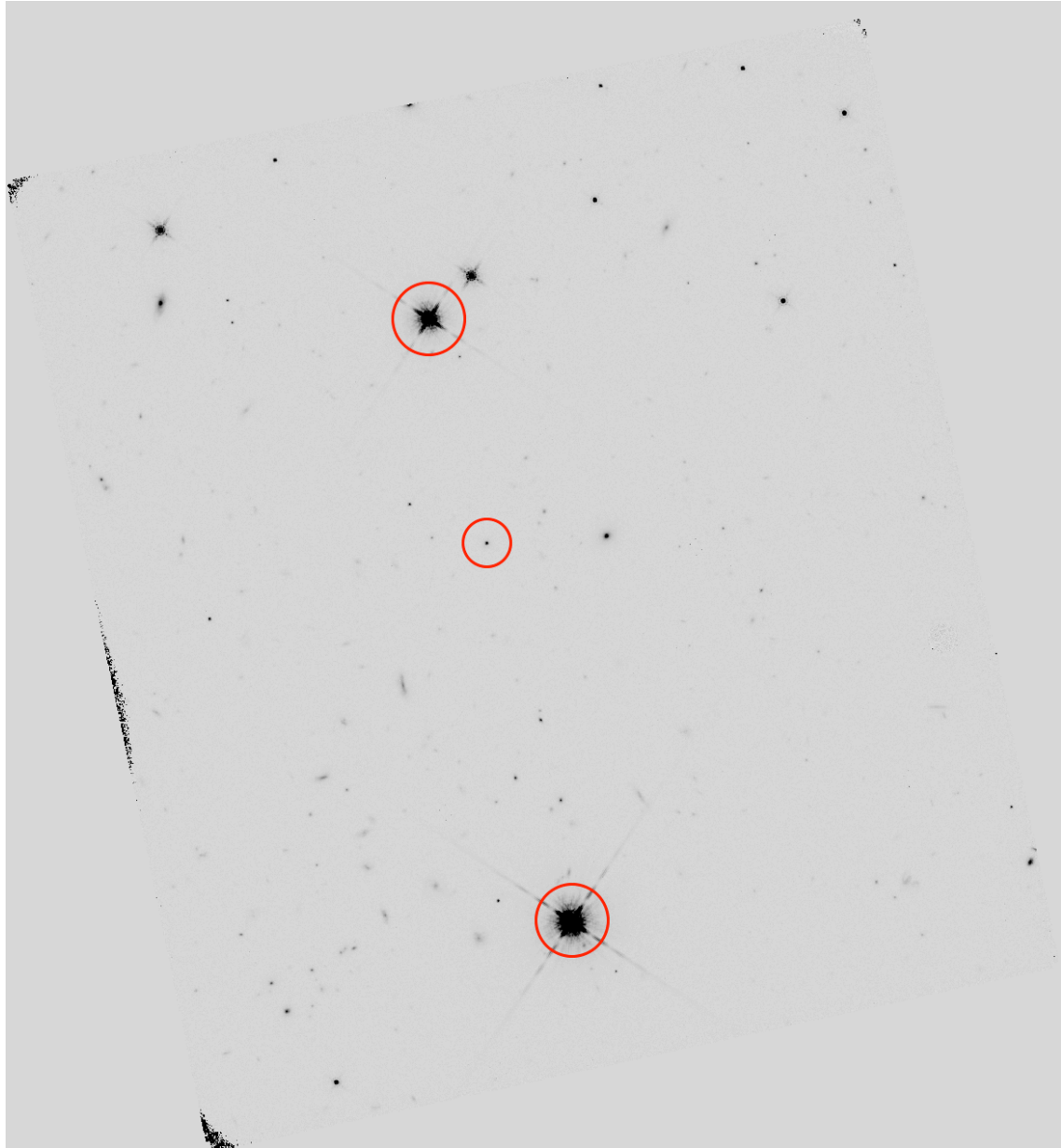


Figure 10: A wide field view of our WFC3 IR channel observations of Sw 1644+57. The image shows the full field of view, and marks the location of two 2MASS and UCAC3 stars used for astrometric calibration (A and B in table 5, as well as the central position of the host galaxy of Sw 1644+57).

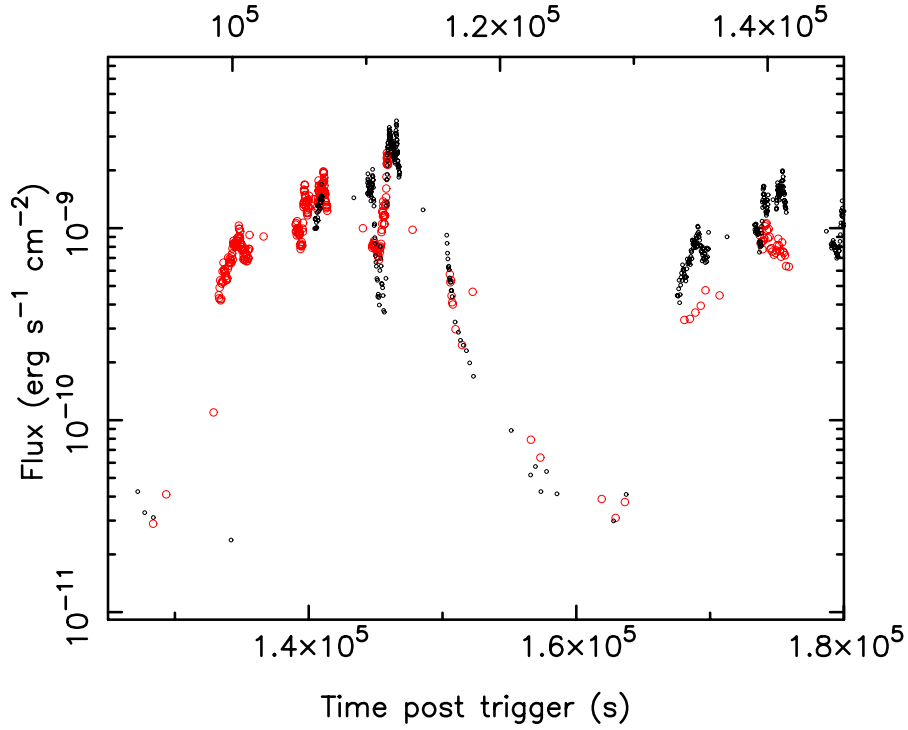


Figure 11: Zoom in of the X-ray light curves of the two bright flares on the second day post-trigger. The earlier flare is plotted in black points and corresponds to the upper time axis, and the later flare in red corresponds to the lower time axis. The fold period is 34300s. Note that there has been no flux normalization applied, such that the peak luminosity of the flares is very similar.

Mid-Time	Interval & duration	Frequency	Flux Density (μJy)
April 1.15	(March 31.904 - April 1.393; 12h int.)	4.8 GHz	990 ± 29
April 4.14	(April 3.897 - 4.375; 5.3h int.)	4.8 GHz	1573 ± 36
April 4.16	(April 3.920 - 4.395; 5.3h int.)	1.4 GHz	221 ± 82
April 10.12	(April 9.880 - 10.359; 5.3h int.)	4.8 GHz	2185 ± 39
April 10.14	(April 9.903 - 10.379; 5.3h int.)	1.4 GHz	284 ± 91

Table 9: A log of observations obtained at the WSRT, showing the times of the observations, their duration, band and measured flux density.

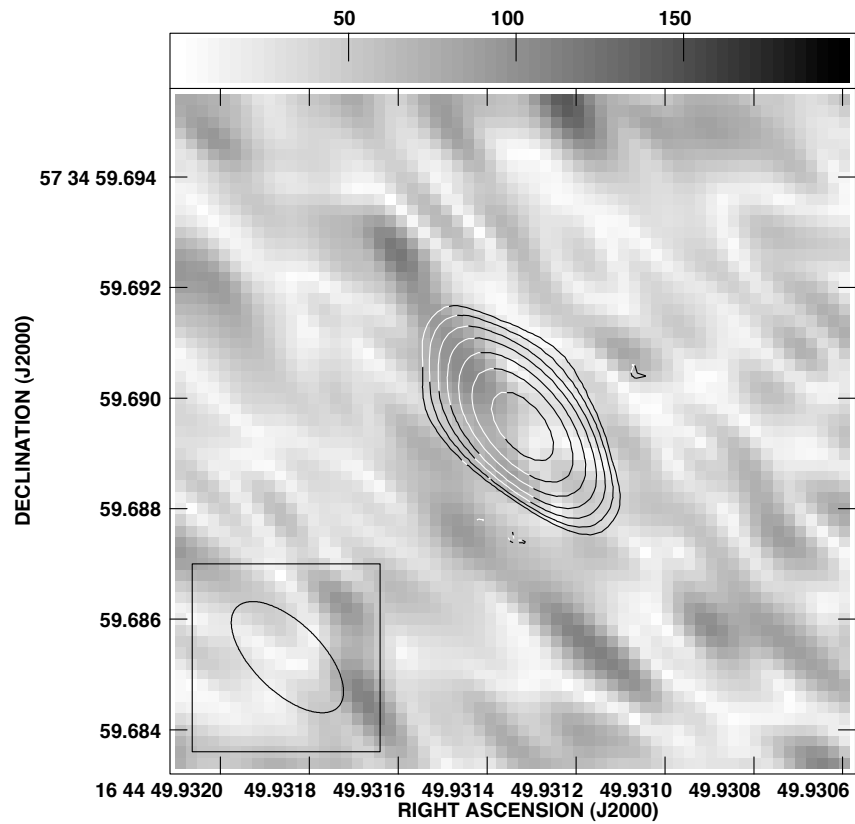


Figure 12: Image of GRB 110328A obtained with the VLBA from 1 and 3 April 2011. The contour levels indicate the Stokes I image, while the gray scale indicates the polarized intensity. Contour levels are -4 , 4 , 5.6 , 8 , 11.2 , 16 , 22.4 , and 32 times the rms noise of 37 microJy. The synthesized beam is shown in the lower left.